6270–6289 *Nucleic Acids Research, 2012, Vol. 40, No. 13* *Published online 20 March 2012*
doi:10.1093/nar/gks234

Mammalian HCA66 protein is required for both ribosome synthesis and centriole duplication

Chrystelle Bonnart[1,2], Marie Gérus[1,2], Coralie Hoareau-Aveilla[1,2], Tamás Kiss[1,2], Michèle Caizergues-Ferrer[1,2], Yves Henry[1,2] and Anthony K. Henras[1,2,*]

[1]Centre National de la Recherche Scientifique, Laboratoire de Biologie Moléculaire Eucaryote and [2]Université de Toulouse, UPS, F-31000 Toulouse, France

Received June 22, 2011; Revised February 21, 2012; Accepted February 28, 2012

ABSTRACT

Ribosome production, one of the most energy-consuming biosynthetic activities in living cells, is adjusted to growth conditions and coordinated with the cell cycle. Connections between ribosome synthesis and cell cycle progression have been described, but the underlying mechanisms remain only partially understood. The human HCA66 protein was recently characterized as a component of the centrosome, the major microtubule-organizing center (MTOC) in mammalian cells, and was shown to be required for centriole duplication and assembly of the mitotic spindle. We show here that HCA66 is also required for nucleolar steps of the maturation of the 40S ribosomal subunit and therefore displays a dual function. Overexpression of a dominant negative version of HCA66, accumulating at the centrosome but absent from the nucleoli, alters centrosome function but has no effect on pre-rRNA processing, suggesting that HCA66 acts independently in each process. In yeast and HeLa cells, depletion of MTOC components does not impair ribosome synthesis. Hence our results suggest that both in yeast and human cells, assembly of a functional MTOC and ribosome synthesis are not closely connected processes.

INTRODUCTION

Early steps of ribosome synthesis in the nucleoli of eukaryotic cells begin with the synthesis by RNA polymerase I of a pre-ribosomal RNA (pre-rRNA) containing the sequences of three of the four mature rRNAs (18S, 5.8S and 25S/28S) separated by spacer regions. This nascent pre-rRNA assembles co-transcriptionally with a subset of ribosomal proteins, with the fourth rRNA (5S) and with numerous small nucleolar ribonucleoprotein particles (snoRNPs) and trans-acting factors to generate the 90S pre-ribosomal particle or small subunit (SSU) processome. This early particle undergoes a complex maturation pathway during which the pre-rRNA is chemically modified at specific nucleotides, processed by endonucleolytic cleavages and exonucleolytic degradations and progressively assembled with ribosomal proteins. This maturation results in a complex series of pre-ribosomal particles which progressively transit from the nucleolus toward the nucleoplasm and get exported through the nuclear pore complexes. The final maturation events occurring in the cytoplasm release the functional ribosomal subunits that perform protein synthesis [for recent reviews, see (1–3)].

Ribosome synthesis is tightly adjusted to growth conditions and coordinated with cell cycle progression. Several aspects of the connections between ribosome synthesis and the cell cycle have been described. In most eukaryotes, RNA polymerase I activity is inhibited at the metaphase stage of mitosis (4) and it was shown more recently that in yeast cells, rDNA transcription is reduced during anaphase (5). In addition, both in yeast and mammalian cells, ribosome synthesis seems to be monitored during the G1 phase of the cell cycle by a surveillance mechanism ensuring that defects in this process inhibit passage through the G1/S transition. In yeast, depletion of factors required for ribosome biogenesis delays the G1/S transition (called 'Start') before it affects the steady-state accumulation of mature ribosomes (6,7). This effect seems to be mediated by Whi5p, a negative regulator of the Start transition (6). Similarly, inactivation of mouse factors required for synthesis of the large ribosomal subunit induces a p53-dependent cell cycle arrest in G1 (8–12). In various human cell lines, inhibition of RNA polymerase I (13–16), or RNAi-mediated knockdown of genes encoding ribosomal proteins (17–20) or ribosome assembly factors (21–28) elicit p53 accumulation and

*To whom correspondence should be addressed. Tel: +33 5 61 33 59 55; Fax: +33 5 61 33 58 86; Email: henras@biotoul.fr

The authors wish it to be known that, in their opinion, the first two authors should be regarded as joint First Authors.

block cell cycle progression in G1. The current model proposes that under conditions of unproductive ribosome synthesis, several ribosomal proteins and assembly factors become less mobilized into the pre-ribosomal particles and accumulate as free proteins in the nucleoplasm where they inhibit the p53 ubiquitin ligase MDM2. This results in p53 stabilization and cell cycle arrest in G1 [for a recent review, see (29)].

Another aspect of the connections between ribosome synthesis and cell cycle progression is that several ribosome synthesis factors have been shown to be directly required for proper progression of mitosis in yeast and mammals. In yeast, conditional mutations in the genes encoding several factors required for the maturation of the large ribosomal subunit such as Ebp2p (30), Rrb1p (31), Rrp14p (32) and Nop15p (33), induce cell cycle arrests at different stages of mitosis. The mitotic defects observed in the absence of these factors are presumably not indirect consequences of impaired translation since the stages affected vary depending on the mutation and since the defects appear rapidly after transfer of the mutant cells to restrictive conditions and therefore very probably precede the depletion of functional ribosomes (31,33). Another such example is the MRP ribonucleoprotein particle catalyzing the endonucleolytic cleavage of the pre-rRNA at site A_3 and also required for proper exit from mitosis (34–36). In mammalian cells, nucleophosmin/B23 and nucleolin have been shown to be required for centrosome duplication and chromosome segregation in mitosis in addition to their role in ribosome biogenesis (37,38). Taken together, these data suggest that several factors involved in ribosome synthesis also directly participate in progression through specific stages of mitosis. These factors may mediate a connection between ribosome synthesis and mitosis or function independently in these two processes. Whatever the biological significance of these dual functions, complex communications seem to take place between ribosome synthesis and cell cycle progression, but the exhaustive list of factors and mechanisms involved remains to be defined.

In addition to its role in the activation of apoptosis (39), the human HCA66 protein has recently been characterized as a component of the pericentriolar material required for the stability of the gamma-tubulin small complex (γ-TuSC) at the centrosome, the major microtubule-organizing centre (MTOC) in mammalian cells (40). Depletion of HCA66 inhibits centriole duplication and induces abnormal spindles in mitosis. Interestingly, HCA66 also localizes to the nucleoli and we show here that it is required for production of the mature 18S rRNA in HeLa cells. HCA66 is therefore a novel factor required for both ribosome synthesis and centriole duplication in human cells. The homologue of HCA66 in *Saccharomyces cerevisiae*, Utp6p, is required for the synthesis of the 18S rRNA (41,42). We show that some aspects of the precise molecular function of HCA66/Utp6p in ribosome synthesis are conserved in yeast and mammals. In yeast cells however, Utp6p is likely not required for the duplication of the MTOC. Alteration of the function of HCA66 at the centrosome in HeLa cells does not inhibit the maturation of the pre-rRNAs, suggesting that some aspects of centrosome assembly and ribosome synthesis are not connected and that HCA66 acts independently in these two processes.

MATERIALS AND METHODS

Plasmid constructions

Plasmid *pEGFP-HCA66* has been described previously (40). The *pEGFP-HCA66*$_{A99E}$, *pEGFP-HCA66*$_{H137A}$, *pEGFP-HCA66*$_{E153A}$, *pEGFP-HCA66*$_{R170A}$ and *pEGFP-HCA66*$_{K102A–D106A}$ were generated by site-directed mutagenesis as follows. Complementary primers were designed to insert single or double mutations by PCR in the *HCA66* ORF sequence of the *pEGFP-HCA66* plasmid. For each mutagenesis, the PCR reaction mix contained 25 ng of *pEGFP-HCA66* plasmid, 13 nmol of each dNTP, 10 pmol of each mutagenic primer, 2.5 U of Pfu Turbo DNA polymerase AD (Stratagene) and 1 × reaction buffer in a final volume of 50 µl. The mutagenic primer couples were OCB43/44, OCB45/46, OCB47/48, OCB49/50 and OCB51/52 (Supplementary Table S1), allowing introduction of the A99E, E153A, H137A, K102A-D106A and R170A substitutions, respectively, in the corresponding modified proteins. The PCR program was the following: a denaturation step at 95°C for 1 min was followed by 18 cycles of denaturation (95°C, 50 s), annealing (60°C, 1 min) and polymerization (68°C, 14 min) and a final extension step at 68°C during 10 min was added. Forty microliters of the PCR reactions were then incubated with 3 µl DpnI enzyme (20 U/µl, New England Biolabs) for 1 h at 37°C. One-twentieth of the DpnI-digested PCR mixes was transformed into DH5α competent cells. Plasmid DNAs were extracted from recombinant clones and the presence of the mutations was verified by sequencing.

To generate plasmid *p3XFLAG-WDR36*, the *WDR36* ORF was amplified by PCR using a plasmid containing the fully sequenced *WDR36* cDNA (purchased from Open Biosystems, clone ID: 9020507) and primers OHA378 and OHA379 (Supplementary Table S1), allowing insertion of EcoRI and BamHI sites upstream and downstream, respectively, of the PCR fragment. The resulting product was digested by EcoRI and BamHI and cloned into *p3XFLAG-CMV-10* (Clontech) digested by the same enzymes.

To generate plasmid *pRWP-SpUtp6-mCherry*, the *SPBC244.02c* ORF sequence was cloned in frame with the mCherry coding sequence into the *Schizosaccharomyces pombe* pRWP expression vector (43). The mCherry coding sequence was amplified by PCR from plasmid pRSET-B-mCherry (kindly provided by J. Rech and D. Lane, LMGM, Toulouse) using OCB75 and OCB76 primers (Supplementary Table S1), allowing insertion of BamHI and BglII restriction sites upstream and downstream, respectively, of the mCherry sequence. The resulting PCR product was digested by BamHI and BglII restriction enzymes and inserted into the pRWP plasmid digested by BamHI, generating plasmid *pRWP-mCherry*. The *SPBC244.02c* ORF sequence was amplified by PCR from a sample of *S. pombe* genomic

DNA (kindly provided by M. Faubladier, LBME Toulouse) using OCB73 and OCB74 primers (Supplementary Table S1), allowing insertion of XhoI and BamHI restriction sites upstream and downstream, respectively, of the ORF sequence. The resulting PCR product was cloned into *pRWP-mCherry* plasmid upstream of the mCherry sequence using the XhoI and BamHI restriction sites.

HeLa cell culture and transfections

HeLa cells were grown in DMEM (Gibco) supplemented with 10% fetal bovine serum (Gibco), 1 mM sodium pyruvate (Gibco), 10 U/ml penicillin and 10 µg/ml streptomycin (Gibco) at 37°C with 5% CO_2.

Transfections of siRNAs described in Figures 1C and 2 were performed as follows. HeLa cells were collected by trypsinization, rinsed with sterile ZAP buffer (10 mM Sodium Phosphate pH 7.25, 250 mM sucrose, 1 mM $MgCl_2$) and resuspended at a density of 5×10^7 cells/ml in ZAP buffer. Two hundred microliters of cell suspension (10^7 cells) were incubated 5 min on ice, mixed with 1 nmol of siRNA duplex, transferred into 4 mm cuvettes (Eurogentec) and cells were electro-transformed with a Bio-Rad Gene Pulser apparatus (square wave protocol, 10 pulses of 5 ms at 240 V separated by 1-s intervals). Transfected cells were immediately mixed with 200 µl of pure fetal bovine serum (Gibco), incubated 3 min at room temperature, resuspended in 10 ml of supplemented DMEM (see above) and plated.

For transfection experiments presented in Figures 1A, 3 and 7, 10^7 HeLa cells resuspended in 200 µl Opti-MEM (Gibco) were mixed with 10 µg of plasmid DNA or 1 nmol of siRNA duplex. The samples were transferred into 4 mm cuvettes (Eurogentec), incubated 5 min on ice and cells were electro-transformed with a Bio-Rad Gene Pulser apparatus (Exponential protocol, 250 V, 950 µF). Cells were immediately recovered, resuspended in 10 ml of supplemented DMEM (see above) and plated.

For co-transfection experiments presented in Figure 6, 10^7 HeLa cells resuspended in 200 µl Opti-MEM (Gibco) were electro-transformed with 10 µg of plasmid DNA and 1 nmol of siRNA duplex as described earlier.

For the immunoprecipitation experiments presented in Figure 6, HeLa cells contained in one 14-cm dish at ~60% confluence were transfected with 10 µg of each plasmid using jetPRIME reagent (Polyplus transfection) and following the manufacturer's protocol.

Saccharomyces cerevisiae strains and media

All yeast strains used in this study were derivatives of *S. cerevisiae* strain BY4741 (*MAT*a *his3Δ1 leu2Δ0 met15Δ0 ura3Δ0*).

Strain *SPC97::GFP* was derived from strain *SPC97::TAP* (Open Biosystems) by replacement of the *TAP* cassette and *HIS3MX6* marker by a *GFP* cassette and *KlURA3* marker as follows. A cassette containing the GFP tag sequence and the *KlURA3* selectable marker was amplified by PCR from plasmid *pFA6a-GFP(S65T)-KlURA3* (44) using oligonucleotides F2long and R1long (Supplementary Table S1). This cassette was inserted by homologous recombination in place of the *TAP* cassette and the *HIS3MX6* marker in strain *SPC97::TAP*.

To generate strain *UTP6::3HA; SPC97::GFP*, we first constructed strain *UTP6::3HA* as follows. A cassette containing the 3HA tag sequence and the *kanMX6* selectable marker was amplified by PCR from plasmid *pFA6a-3HA-kanMX6* using oligonucleotides OHA262 and OHA241 (Supplementary Table S1). This cassette was inserted by homologous recombination downstream of the chromosomal *UTP6* ORF in strains BY4741 as described (45). A cassette containing the 3HA tag sequence and the *kanMX6* selectable marker flanked by upstream and downstream sequences specific to the *UTP6* chromosomal locus was subsequently amplified by PCR using genomic DNA extracted from strain *UTP6::3HA* and oligonucleotides OHA263 and OHA242 (Supplementary Table S1). This cassette was inserted by homologous recombination at the chromosomal *UTP6* locus in the previously described *SPC97::GFP* strain.

Strains *GAL::3HA::UTP6* and *GAL::3HA::SPC97* were constructed as follows. Cassettes containing the *kanMX6* selectable marker followed by the *GAL1* promoter and the 3HA tag sequence were amplified by PCR using plasmid *pFA6a-kanMX6-PGAL1-3HA* (45) and oligonucleotide pairs OHA226/OHA227 (*UTP6*) or OHA306/OHA307 (*SPC97*). These cassettes were inserted by homologous recombination upstream of the chromosomal *UTP6* or *SPC97* ORFs in the BY4741 strain.

Saccharomyces cerevisiae strains were grown either in YP medium (1% yeast extract, 1% peptone) (Becton–Dickinson) supplemented with 2% galactose or 2% glucose as the carbon source (rich medium) or in YNB medium [0.17% yeast nitrogen base (MP Biomedicals), 0.5% $(NH_4)_2SO_4$] supplemented with 2% galactose or 2% glucose and the required amino acids (minimal medium). Selection of the kanamycin-resistant transformants was achieved by addition of G418 to a final concentration of 0.2 mg/ml.

Schizosaccharomyces pombe strains and media

The *S. pombe* strain used in Figure 4 was obtained by transformation of a strain expressing Cdc11-GFP (46,47), kindly provided by Y. Gachet and S. Tournier (LBCMCP, Toulouse) with plasmid *pRWP-SpUtp6-mcherry* as described (48).

Schizosaccharomyces pombe strains were grown either in YES medium supplemented with 2% glucose as the carbon source and amino acids at 225 mg/l (rich medium) or in MM medium supplemented with 2% glucose and the required amino acids (minimal medium). Repression of SpUtp6-mCherry expression was achieved by addition of thiamine to a final concentration of 4 µM.

Protein extractions and western-blot analyses

Western-blot analyses of protein samples resulting from HeLa cell fractionation experiments (Figure 1B) were performed as follows. All the soluble fractions obtained at the different steps of the fractionation experiment (see 'HeLa

cell fractionations' section) were mixed with one volume of 2 × gel-loading buffer (100 mM Tris–HCl pH 6.8, 4% SDS, 20% glycerol, 200 mM dithiothreitol, 0.2% bromophenol blue). The nucleolar insoluble material was resuspended with 1 × gel-loading buffer and subjected to three pulses of sonication at 4°C (15 s each separated by 30-s incubations on ice) using a Bioruptor (Diagenode) set at level high. The proportion of the different fractions analyzed by western blot was as follows: Total (1/3000); Cytoplasm (1/1000); Nuclei (1/500); Nucleoplasm (1/500); Nucleolar soluble fraction (1/40); Nucleolar insoluble fraction (1/40). Samples were heated 10 min at 65°C, loaded on a NuPAGE 4–12% Bis–Tris Gel (Invitrogen) and transferred to Amersham Hybond-C Extra membranes (GE Healthcare).

Total protein extractions from HeLa cells (Figures 2A and 3A) were performed as follows. HeLa cells were washed twice with ice-cold PBS, scrapped in ice-cold PBS, recovered by centrifugation and resuspended with a buffer containing 20 mM Tris–HCl pH 7.4, 150 mM NaCl, 10 mM EDTA, 10% glycerol and 1% NP40 supplemented with complete protease inhibitor cocktail (Roche). Cells were then disrupted by three pulses of sonication at 4°C (30 s each separated by 30-s incubations on ice), using a Bioruptor (Diagenode) set at level high. Insoluble material was eliminated by centrifugation at 13 000 rpm for 5 min (4°C) and protein concentrations of the soluble extracts were determined using Bradford assay. Thirty micrograms of proteins were mixed with 1 × gel-loading buffer (50 mM Tris–HCl pH 6.8, 2% SDS, 10% glycerol, 100 mM dithiothreitol, 0.1% bromophenol blue), heated at 95°C for 5 min and loaded on SDS–10% polyacrylamide gels. Proteins were transferred to Amersham Hybond-C Extra membranes (GE Healthcare).

Total protein extracts from yeast cells were prepared as described (49). Samples were heated 15 min at 65°C, loaded on SDS–10% polyacrylamide gels and transferred to Amersham Hybond-C Extra membranes (GE Healthcare).

For all western-blot experiments except those using anti-HCA66 antibodies, membranes were saturated for 1 h with PBST buffer (137 mM NaCl, 2.7 mM KCl, 10 mM Na_2HPO_4, 2 mM KH_2PO_4, 0.1% Tween-20) containing 5% (w/v) powder milk, incubated for 2 h with the same buffer containing the primary antibodies, rinsed three times for 5 min with PBST buffer containing 1% (W/V) powder milk, incubated for 1 h with the secondary antibodies diluted in PBST containing 1% (w/v) powder milk and finally washed three times for 10 min with PBST buffer. For experiments using anti-HCA66 antibodies, membranes were processed as described earlier except that PBST buffer containing 10% (w/v) powder milk, 1% BSA, 1% NP-40 and 0.5% Tween-20 was used for saturation and for incubations with the primary and secondary antibodies. For experiments using HRP-conjugated anti-HA antibodies, membranes were saturated for 1 h with PBST buffer containing 5% (w/v) powder milk, incubated for 2 h with the same buffer containing the antibodies and finally washed three times for 10 min with PBST buffer. Final detections were performed using regular enhanced chemiluminescence (ECL) western blotting detection reagents (GE Healthcare).

Primary antibodies used to detect the proteins analyzed in this study were the following: anti-HCA66 (40) diluted to 1:400; anti-HDAC2 (monoclonal clone 3F3, Santa Cruz Biotechnology, kindly provided by K. Bystricky, LBME, Toulouse) diluted to 1:1000; anti-nucleolin (kindly provided by P. Bouvet, ENS, Lyon) diluted to 1:750; anti-GFP rabbit polyclonal antibodies (kindly provided by M. Faubladier and P.E. Gleizes, LBME, Toulouse) diluted to 1:5000; anti-actin (monoclonal clone C4, Millipore) diluted to 1:10 000; anti-HA (clone 3F10; Roche) diluted to 1:1000; anti-Nhp2 rabbit polyclonal antibodies (50) diluted to 1:5000; anti-FLAG M2 (Sigma, F3165) diluted to 1:1000; anti-hnRNP A1 (4B10, Santa Cruz Biotechnology, sc-32301) diluted to 1:2000.

RNA interference

The siRNA duplex targeting the ORF of *HCA66* mRNA was described previously (40). A second siRNA duplex (OCB-si#1sense and OCB-si#1antisense) targeting the first 19 nt of the 3′-UTR of *HCA66* mRNA was used in co-transfection experiments (Supplementary Table S1). The siRNA duplex used to interfere with NEDD1 expression was described previously (51). Negative control siRNAs (scrambled siRNAs) were purchased from Eurogentec (SR-CL000-005). All siRNA duplexes were transfected as described in 'HeLa cell culture and transfections'.

RNA extractions and Northern-blot experiments

Extractions of total RNAs from HeLa cells (Figures 2B, 3B, 6B and 7D) were performed using Trizol reagent (Invitrogen). Equal amounts of total RNAs (4 μg) were analyzed by Northern blot (see below).

For the pulse chase experiment, total RNAs were extracted using Trizol reagent (Invitrogen) and RNA samples corresponding to equal amounts of cells were analyzed by Northern blot.

Extractions of total RNAs from yeast cells (Figure 5C) were performed as described (52). Equal amounts of total RNAs (4 μg) were analyzed by Northern blot (see below).

For Northern-blot analyses of low molecular weight species (Figure 2B, 5S and 5.8S rRNAs), 4 μg of total RNAs were separated on polyacrylamide gels (6% acrylamide:bisacrylamide [19:1], 8 M urea, 1 × Tris–borate–EDTA buffer). For Northern-blot analyses of higher molecular weight species (Figures 2B, 5C, 6B and 7D), 4 μg of total RNAs were separated as described in 'Molecular Cloning', Sambrook and Russell, CSHL Press ('Separation of RNA According to Size: Electrophoresis of Glyoxylated RNA through Agarose Gels'). RNAs were transferred to Amersham Hybond-N (low molecular weight species) or Hybond-N^+ (high molecular weight species) membranes (GE Healthcare) which were hybridized with ^{32}P-labeled oligonucleotides using Rapid-hyb buffer (GE Healthcare). Signals were detected by autoradiography. The sequences of the oligonucleotides used as probes in this study are described in Supplementary Table S1.

Pulse chase analysis

HeLa cells were electro-transformed with the siRNA duplex targeting the ORF of *HCA66* mRNA as described in the 'RNA interference' section. Cells were then grown on 12-well plates for 48 h. The pulse chase protocol was adapted from (53). Cells were incubated in methionine-free DMEM (Invitrogen) for 30 min at 37°C, labeled for 15 min with L-methyl ^{3}H methionine (50 μCi/ml), rinsed with regular DMEM and incubated for 0 (immediately rinsed with ice-cold PBS), 7.5, 15, 30, 60 and 90 min in regular DMEM. Cells were rinsed with ice-cold PBS and immediately resuspended directly with 500 μl Trizol reagent (Invitrogen) for RNA extractions. Purified RNAs were separated on a 1.2% agarose gel and transferred to Amersham Hybond N^{+} membranes (GE Healthcare) as described earlier. The membranes were exposed for several days to Biomax KODAK™ MS films through a KODAK™ BioMax® TranScreen LE.

HeLa cell fractionations

A HeLa cell nuclear extract was prepared as follows using the 'Nucleolar Isolation Protocol' available on the Lamond laboratory website (http://www.lamondlab.com/f7protocols.htm). Unless stated otherwise, all steps were performed at 4°C and all solutions were kept at 4°C and contained 0.5 U/μl of RNasin (Promega) and 1 × complete protease inhibitor cocktail (Roche). About 1.4×10^{8} exponentially growing HeLa cells were trypsinized and washed with buffer A (10 mM HEPES pH 7.9, 10 mM KCl and 1.5 mM $MgCl_2$). Cells were then mechanically disrupted with a Dounce homogenizer in Buffer A supplemented with 0.5 M dithiothreitol. After centrifugation at 1000*g* for 10 min, the supernatant (i.e. cytoplasmic fraction) was removed and saved for western-blot analysis and the pellet (i.e. nuclei) was washed with a buffer containing 10 mM Tris–HCl pH 7.5, 3.3 mM $MgCl_2$ and 250 mM sucrose. After centrifugation at 120*g* for 5 min, the nuclei were resuspended with a solution containing 10 mM $MgCl_2$, 250 mM sucrose and further purified by centrifugation at 500*g* for 10 min on a sucrose cushion (0.5 mM $MgCl_2$, 350 mM sucrose). Nuclei were resuspended with a buffer containing 0.5 mM $MgCl_2$ and 350 mM sucrose and disrupted by seven pulses of sonication at 4°C (15 s each separated by 30-s incubations on ice) using a Bioruptor (Diagenode) set at level high. An aliquot of the resulting material was saved for western-blot analysis (total nuclei). The nucleolar fraction was separated from the nucleoplasmic fraction by centrifugation at 2000*g* for 10 min (4°C) on a sucrose cushion (0.5 mM $MgCl_2$, 880 mM sucrose). After centrifugation, the nucleoplasmic extract is concentrated in the milky, upper part of the fraction, while nucleoli are in the pellet. The pellet was washed with a buffer containing 10 mM Tris–HCl pH 7.4, 2.5 mM $MgCl_2$ and 20 mM KCl. After centrifugation at 1500*g* for 5 min (4°C), the pellet was resuspended with a buffer containing 10 mM Tris–HCl pH 7.4, 10 mM NaCl and 10 mM dithiothreitol. Nucleoli were incubated 45 min at 15°C in this buffer before a final sonication step at 4°C (two pulses of 10 s each separated by 30-s incubations on ice, Bioruptor, level high). The soluble nucleolar fraction was separated from the insoluble nucleolar material by centrifugation at 10 000*g* for 10 min (4°C).

Sedimentation on sucrose gradient

Approximately 2×10^{7} exponentially growing HeLa cells were electroporated with *HCA66* or scrambled siRNAs as described in 'HeLa cell culture and transfections'. Three days after electroporation, culture medium was removed and fresh, 37°C-prewarmed medium was added to the cells. After an incubation of ~90 min at 37°C, cycloheximide was added directly to the culture medium at a concentration of 10 μg/ml and incubation was prolonged for 10 min. Cells were harvested by trypsinization and washed two times with PBS (cycloheximide was added at a concentration of 100 μg/ml to PBS and trypsin). The cell pellet was then washed with buffer A (10 mM HEPES–KOH pH 7.9, 10 mM KCl, 1.5 mM $MgCl_2$, 100 μg/ml cycloheximide) and then incubated in 1 ml of the same buffer supplemented with 0.5 mM dithiothreitol, 1 × Complete EDTA-free protease inhibitor cocktail (Roche) and 0.5 U/μl RNasin (Promega). Cells were incubated on ice for 20 min and disrupted using a Dounce homogenizer with a tight pestle. Cells were then centrifuged at 1000*g* for 5 min at 4°C, in order to pellet nuclei. The top soluble phase, containing the cytoplasmic fraction, was clarified through one centrifugation at 10 000*g* for 5 min at 4°C and quantified by measuring absorbance at 260 nm. Approximately 20 A_{260} units were loaded on a 4.5–45% sucrose gradient in buffer A (without cycloheximide). Gradients were centrifuged at 39 000 rpm for 2.5 h at 4°C in an Optima L-100XP Ultracentrifuge (Beckman–Coulter) using the SW41Ti rotor without brake. Following centrifugation, the fractions were collected using a Foxy Jr fraction collector (Teledyne ISCO) and the absorbance at 254 nm was measured with a UA-6 device (Teledyne ISCO).

Flow cytometry analyses

FACS analyses using HeLa cells (Figure 7A) were performed as follows. HeLa cells transfected with the vectors encoding EGFP, EGFP-HCA66, EGFP-$HCA66_{1–86}$ or mock-transfected were grown for 48 h and total cells (adherent and floating) were harvested, counted, washed two times with PBS and resuspended with PBS at a density of 3.3×10^{6} cells/ml (10^{6} cells in 300 μl). Eight hundred microliters of 100% ethanol were slowly added to 300 μl of cell suspensions and cells were fixed overnight at 4°C on a rocking table. Cells were centrifuged at 300*g* for 5 min (4°C) and resuspended with PBS supplemented with 50 μg/ml propidium iodide (Sigma) and 100 μg/ml RNase A (Sigma). Cell samples were analyzed using a FACSCalibur flow cytometer (Becton–Dickinson) and acquisitions were performed using the Cell Quest software (Becton–Dickinson).

FACS analyses using yeast cells (Figure 5B) were performed as follows. About 10^{7} yeast cells growing exponentially were fixed with 70% ethanol during at least 15 min, collected by centrifugation and resuspended with 200 mM

Tris–HCl pH 7.8. Cells were treated with 10 μg/ml RNase A (Sigma) overnight at 37°C, collected by centrifugation and resuspended with a buffer containing 200 mM Tris–HCl pH 7.5, 200 mM NaCl, 78 mM $MgCl_2$. Aggregated cells were dissociated through two series (separated by incubation on ice) of four sonication pulses (Branson Sonifier 250, setting 2 out of 10, 50% output). Cells were collected by centrifugation and resuspended with 500 μl of a buffer containing 180 mM Tris–HCl pH 7.5, 190 mM NaCl, 70 mM $MgCl_2$ supplemented with 55 μg/ml of propidium iodide (Sigma). Twenty microliters of each cell suspension were added to 1 ml of 50 mM Tris–HCl pH 7.8 and 30 000 cells were analyzed with a FACSCalibur (Becton–Dickinson) flow cytometer and acquired with Cell Quest software (Becton–Dickinson). To quantify the proportion of cells in the different phases of the cell cycle, the raw cytometer data were converted to histograms using WinMDI 2.9 (The Scripps Research Institute, San Diego, CA, USA) and these histograms were quantified using Cylchred 1.0.2 software (School of medicine, Cardiff University, UK).

Fluorescence and immunofluorescence microscopy

Immunofluorescence microscopy using HeLa cells presented in Figure 1A was performed as follows. Transfected HeLa cells were grown on microscope cover glasses in 6-well plates for 48 h. Cells were fixed with paraformaldehyde as described earlier. Cover glasses were rinsed two times for 5 min with PBS, permeabilized with 0.4% Triton X-100 in PBS for 5 min and washed two times for 5 min with PBS. Fixed cells were incubated for 1 h with 1% BSA (Sigma A8022) in PBS. Cells were then incubated for 2 h with the same solution containing anti-fibrillarin monoclonal antibodies (clone 72B9) diluted to 1:200 or anti-γ-tubulin monoclonal antibodies (clone GTU-88, Sigma) diluted to 1:500. Cells were washed two times for 5 min with 1% BSA in PBS, and subsequently incubated for 1 h with TRITC-conjugated anti-mouse antibodies (Dako) diluted to 1:200 in PBS containing 1% BSA. Cells were washed three times for 5 min with 1% BSA in PBS, one time with PBS only and cover glasses were mounted in Mowiol-DAPI.

Immunofluorescence microscopy using *S. cerevisiae* cells (Figure 4A) was performed as follows. About 2×10^8 cells growing exponentially were fixed with 4% paraformaldehyde (Electron Microscopy Science) during 30 min under conditions of gentle shaking, collected by centrifugation, rinsed with buffer B (8.6 mM K_2HPO_4, 1.3 mM KH_2PO_4, 1.2 M sorbitol) and collected again by centrifugation. Cell pellets were resuspended with 500 μl of a digestion buffer obtained by mixing 1 ml of buffer B with 10 μl of 200 μM vanadium ribonucleoside complex, 2 μl of 0.1 M phenylmethylsulfonyl fluoride (PMSF, Sigma), 2 μl of 14.3 M β-mercaptoethanol and 10 μl of 5 mg/ml Zymolyase 100T (Seikagaku Corporation). After 45 min at 30°C, spheroplasts were collected by gentle centrifugation, resuspended with 500 μl of buffer B, spotted on eight-well multitest slides previously coated with poly-L-lysine (Sigma) and incubated for 1 h at room temperature to allow cell adhesion. Excess cells were removed, and slides were incubated for 5 min in PBS containing 0.1% BSA (Sigma A8022) and then two times for 5 min in PBS containing 0.1% BSA and 0.1% NP-40. Slides were then incubated for 2 h at room temperature with anti-HA mouse monoclonal antibodies (clone 12CA5, Roche) diluted to 1:200 in PBS containing 0.1% BSA, rinsed once for 5 min with PBS containing 0.1% BSA, once for 5 min with PBS containing 0.1% BSA and 0.1% NP-40 and once again for 5 min with PBS containing 0.1% BSA. Slides were then incubated for 2 h at room temperature with Alexa Fluor 555-conjugated goat anti-mouse IgGs (Invitrogen) diluted to 1:1000 in PBS containing 0.1% BSA. Slides were then rinsed three times as described earlier and mounted in Mowiol-DAPI.

Fluorescence microscopy using *S. pombe* cells (Figure 4B) was performed as follows. Approximately 2×10^8 *S. pombe* cells were fixed with 4% paraformaldehyde (Electron Microscopy Science) during 5 min under conditions of gentle shaking, collected by centrifugation, rinsed three times with PEMS buffer (100 mM PIPES pH 6.9, 1 mM EGTA, 1 mM $MgSO_4$, 1.2 M Sorbitol) and resuspended at 2×10^9 cells/ml. Approximately 6×10^6 cells were spotted on eight-well multitest slides previously coated with poly-L-lysine (Sigma). DNA was counterstained with 0.1 μg/ml DAPI (4′,6-diamidino-2-phenyllindole) in Mowiol.

Images were captured using either a DMRB microscope (Leika) equipped with a Photometrics Roper CoolSNAP ES camera or an inverted IX-81 microscope (Olympus) equipped with a Photometrics Roper CoolSNAP HQ camera, both driven by MetaMorph (Molecular Devices). Fluorescent signals were captured after different exposure times (between 500 and 2000 ms) depending on signal intensities. The exposure times and γ values were adjusted in order to enhance the lowest gray levels, especially for the observations of centrosomal signals in human cells. Image analyses were performed using MetaMorph software.

Immunoprecipitation experiments

HeLa cells contained in one 14-cm diameter dish at ~60% confluence were transfected with vectors allowing expression of EGFP-HCA66 (WT), EGFP-$HCA66_{A99E}$ or EGFP-$HCA66_{K102A/D106A}$ in combination with vectors driving expression of either FLAG-WDR36 or FLAG only (empty vector) as described in 'HeLa cell culture and transfections'. Forty-eight hours after transfection, cells were rinsed with ice-cold PBS, scraped on ice and recovered by centrifugation. Cell pellets were resuspended with 500 μl IP buffer (25 mM Tris–HCl pH 7.5, 5 mM MgAc, 200 mM NaCl, 0.2% Triton X-100) extemporaneously supplemented with 1 mM dithithreitol, 1 × Complete EDTA-free protease inhibitor cocktail (Roche) and 0.1 U/μl RNasin (Promega) and were disrupted by sonication (pulses of 30 s at level medium separated by 30-s incubations on ice during 5 min), using a Bioruptor (Diagenode). Cell extracts were clarified by centrifugation at 16 000*g* and 4°C for 10 min and incubated with 20 μl of anti-FLAG M2 affinity gel (Sigma, A2220) for 90 min at 4°C on a rocking table.

Agarose beads were rinsed six times with 1 ml of IP buffer and were resuspended with 30 µl of 2 × SDS gel-loading buffer (100 mM Tris–HCl pH 6.8, 4% SDS, 20% glycerol, 200 mM dithiothreitol, 0.2% bromophenol blue). Immunoprecipitated proteins were analyzed by western blot.

Cell death assay

HeLa cells transfected with the vectors encoding EGFP, EGFP-HCA66 or EGFP-HCA66$_{1–86}$ or mock-transfected were grown for 48 h and total cells (adherent and floating) were harvested and resuspended with supplemented DMEM. One volume of each cell suspension was mixed with one volume of Opti-MEM (Gibco) containing 0.1% trypan blue. The proportion of dead cells in each population was calculated as the ratio of trypan blue positive cells (i.e. dead cells) over total cells.

DNA shearing assay

HeLa cells transfected with the vectors encoding EGFP, EGFP-HCA66, EGFP-HCA66$_{1–86}$ or mock-transfected were grown for 48 h and total cells (adherent and floating) were harvested and washed two times with PBS. About 10^6 cells were resuspended with a lysis buffer containing 10 mM Tris–HCl pH 8, 100 mM NaCl, 25 mM EDTA, 0.5% SDS and 100 µg/µl proteinase K and incubated overnight at 55°C. Extracts were mixed by inversion with one volume of water-saturated phenol pH 8.0 (MP Biomedicals) and centrifuged at 13 000 rpm for 5 min. Aqueous phases were then mixed by inversion with one volume of water-saturated chloroform and centrifuged at 13 000 rpm for 5 min. One volume of Phenol: Chloroform:Isoamyl alcohol mixture (Sigma) was added to the aqueous phases and the samples were mixed using a vortex for 1 min at full power. Samples were centrifuged at 13 000 rpm for 5 min, the aqueous phases were mixed with 0.1 volume of 3 M NaAc pH 5.2 and 3 volumes of 100% ethanol, incubated 1 h at −80°C and centrifuged at 13 000 rpm for 20 min. Pellets were washed with 70% ethanol, resuspended with 20 µl Milli-Q H_2O and treated with 1 µl of 10 mg/ml boiled RNase A for 1 h at 37°C. One-tenth of each extract was loaded on a 1.5% agarose gel along with a molecular weight ladder (Smart Ladder, Eurogentec). The gel was stained with ethidium bromide and the image was captured using a GelDoc XR Transilluminator apparatus (Bio-Rad).

RESULTS

HCA66 accumulates both at the centrosome and in the nucleoli of HeLa cells and it is required for production of the 40S ribosomal subunit

As reported previously, HCA66 is associated with the centrosome from S phase to mitosis in U2OS cells and is required for centriole duplication and the assembly of the microtubule spindle (40). Interestingly, HCA66 accumulates in the nucleoli in interphase, suggesting that it may also participate in ribosome biogenesis. To confirm and extend these observations, we investigated the sub-cellular localization of HCA66 in HeLa cells. HeLa cells were transfected with a plasmid expressing HCA66 fused at the N-terminus with a variant of the green fluorescent protein (EGFP). As shown in Figure 1A, although a fraction of EGFP-HCA66 co-localizes with γ-tubulin at the centrosome, the majority of the fluorescent signal is detected in the nucleoli stained with anti-fibrillarin antibodies. Cell fractionation experiments confirmed these observations (Figure 1B). Endogenous HCA66 is detectable only in the nuclear fraction and its vast majority is present in purified nucleoli. To get some insights into the potential function of HCA66 in ribosome synthesis, we determined whether RNAi-mediated depletion of HCA66 in HeLa cells perturbs ribosomal subunit accumulation levels. HeLa cells were treated with an siRNA targeting the coding region of *HCA66* mRNA or with a control scrambled siRNA, before analysis of ribosomal profiles on sucrose gradients (Figure 1C). We observed a clear reduction in the accumulation level of 40S ribosomal subunits in *HCA66* siRNA-treated cells, as compared to control cells. This phenotype is correlated with a strong depletion of 80S ribosomes and a parallel increase in the accumulation of free 60S subunits. These results are consistent with a function of HCA66 in the production of small ribosomal subunits in HeLa cells.

HCA66 is required for early cleavages of pre-ribosomal RNA and production of mature 18S rRNA

To dissect the function of HCA66 in 40S ribosomal subunit production, we investigated whether HCA66 depletion in HeLa cells perturbs the maturation of pre-rRNAs. HeLa cells were transfected with *HCA66* siRNAs and harvested 48 h after treatment. Western-blot analysis showed a significant decrease in the accumulation levels of endogenous HCA66 in siRNA-treated cells as compared to control cells, which were either mock-transfected or transfected with scrambled siRNAs (Figure 2A). To study the effect of HCA66 knockdown on the pre-rRNA processing pathway (depicted in Figure 2C), we assessed the accumulation levels of precursor and mature rRNAs by Northern blot (Figure 2B). These analyses revealed that the nascent 45S transcript (detected with probe a) accumulated slightly in siRNA-treated cells compared to control cells, suggesting that early cleavage of the 5′ETS at site 01 (also named A′) is delayed. Consistent with this, we observed a slight accumulation of the 30S^{+1} intermediate (54), a 5′-extended version of the 30S pre-rRNA (see below) resulting from cleavage of the initial 45S transcript at site 2 without prior cleavage at site 01. The 45S′ pre-rRNA (detected with probes b and c) deriving from the 45S species following cleavages at sites 01 and 02 in the 5′ETS and 3′ETS, respectively, also probably accumulated indicating that its maturation was partially inhibited or delayed. Maturation of this pre-rRNA following pathway A consists of cleavages at sites A_0 and 1 in the 5′ETS, generating the 43S and 41S intermediates. Accumulation of the 43S (see below Figure 3) and 41S (Figure 2B) species was significantly reduced in siRNA-treated cells,

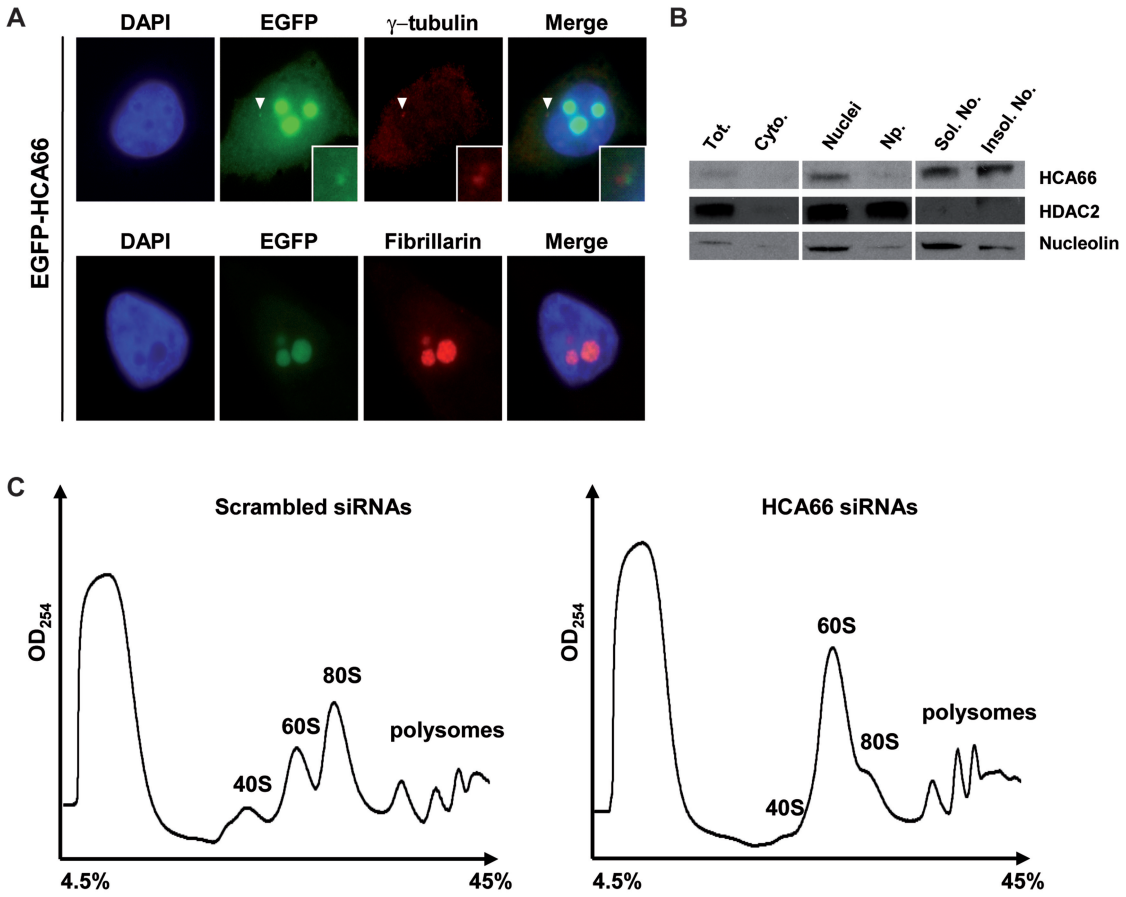

Figure 1. HCA66 is detected both at the centrosome and in the nucleoli in HeLa cells and is required for normal accumulation of 40S ribosomal subunits. (**A**) Immunofluorescence microscopy using HeLa cells expressing EGFP-HCA66 and antibodies detecting γ-tubulin (upper panel) or fibrillarin (lower panel). Scale bar, 10 μm. (**B**) Western-blot analysis of endogenous HCA66 distribution in HeLa cell subcellular fractions. The different lanes correspond to the total extract (Tot.) or the cytoplasmic (Cyto.), nuclear (Nuclei), nucleoplasmic (Np.), soluble nucleolar (Sol. No.) or insoluble nucleolar (Insol. No.) fractions. HDAC2 and nucleolin are markers of the nucleoplasmic and nucleolar material, respectively. (**C**) Sucrose gradient analysis of ribosomal subunit levels in HeLa cells treated with *HCA66* siRNAs. Cytoplasmic extracts prepared from HeLa cells treated with *HCA66* or scrambled siRNAs were centrifuged trough 4.5–45% sucrose gradients. Fractions were collected and the absorbance at 254 nm was measured during collection.

indicating that HCA66 is required for efficient removal of the 5′ETS following cleavage at site 01. In contrast, synthesis of the 30S (detected with probe b) and 32S (detected with probe c) intermediates resulting from cleavage of the 45S′ precursor at site 2 within ITS1 (pathway B) was not inhibited and the accumulation levels of the 30S species was even strongly increased. This profile suggested that HCA66 is not required for cleavage at site 2 but is important for the maturation of the 30S intermediate. This maturation initially consists in the removal of the 5′ETS through cleavages at sites A_0 and 1, generating the 26S and 21S precursors (detected with probe b) respectively. The accumulation levels of both species were significantly reduced in siRNA-treated cells, confirming that HCA66 is required for these processing events. As a consequence, production of the 18S-E intermediate and its direct processing product, the mature 18S rRNA, was affected whereas the synthesis of the mature 28S, 5.8S and 5S rRNAs remained unchanged.

The pre-rRNA processing defects resulting from HCA66 knockdown were further analyzed using pulse-chase experiments (Figure 3). The results confirmed a significant delay in the maturation of the 45S, 45S′ and 30S pre-rRNAs in siRNA-treated cells, and defects in the production of all the species resulting from cleavages at sites A_0 and 1 within the 5′ETS, namely the 43S, 41S and 21S intermediates. As a consequence, synthesis of the 18S-E pre-rRNA and the mature 18S rRNA was delayed, whereas synthesis of the 32S intermediate and the mature 28S rRNA remained unchanged. Altogether, the data presented in Figures 2 and 3 show that HCA66 is required for the processing events leading to the elimination of the 5′ETS spacer of the pre-rRNA, and thereby for production of the 18S rRNA and the 40S ribosomal subunit.

To further understand the role of HCA66 in early steps of ribosome synthesis, we investigated the consequences of HCA66 depletion on the localization of fibrillarin and WDR36, two factors involved in the maturation of pre-ribosomal particles. WDR36 (55) is the homologue of yeast Utp21p which interacts with Utp6p and is another component of the UTP-B module of 90S

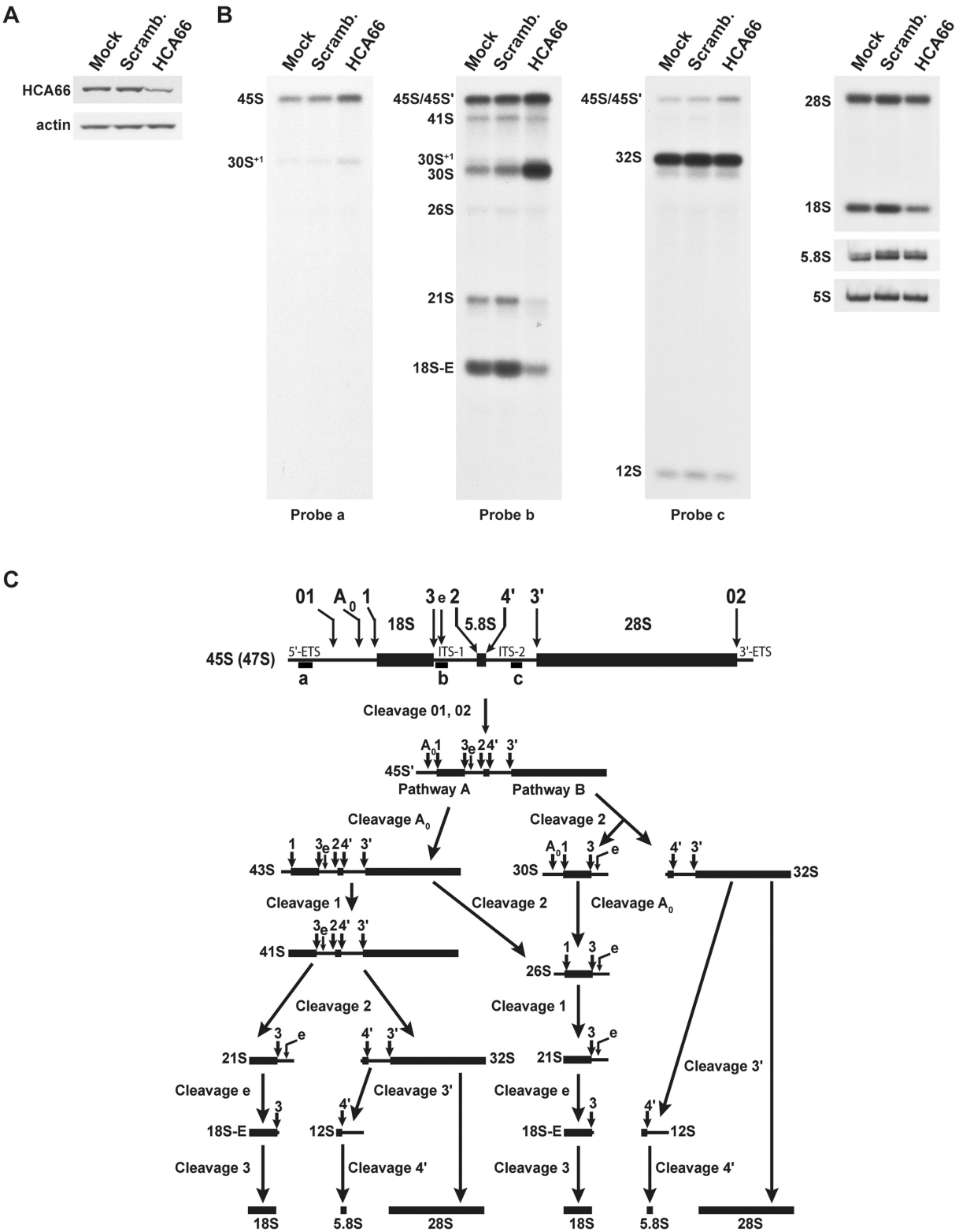

Figure 2. Depletion of HCA66 in HeLa cells affects early cleavages of the pre-rRNA and the production of the mature 18S rRNA. (**A**) Western-blot analysis showing the accumulation levels of endogenous HCA66 and actin (loading control) in HeLa cells 48 h after transfection with H_2O (mock), scrambled siRNAs (Scramb.) or *HCA66* siRNAs (HCA66). (**B**) Northern-blot analysis showing the accumulation levels of the (pre-)rRNAs in HeLa cells 48 h after transfection with H_2O (mock), scrambled siRNAs (Scramb.) or *HCA66* siRNAs (HCA66). The probes used to detect the different species (described in Figure 2C and Supplementary Table S1) are indicated below each panel. (**C**) Outline of the pre-rRNA processing pathway in HeLa cells. Positions of the oligonucleotide probes used in this study (a–c) are indicated and their sequences are described in Supplementary Table S1.

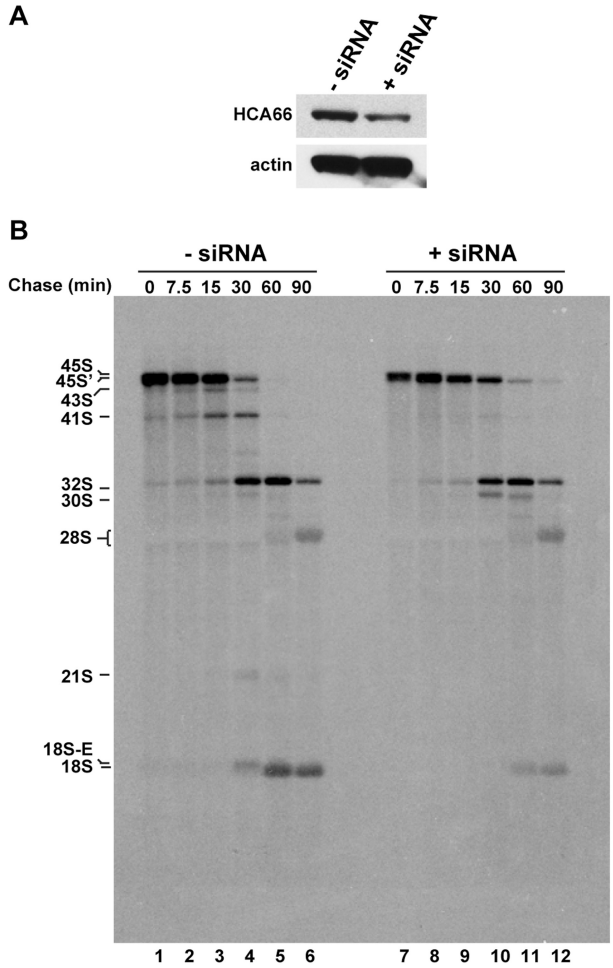

Figure 3. Depletion of HCA66 in HeLa cells delays the production of the mature 18S rRNA. (**A**) Western-blot analysis showing the accumulation levels of endogenous HCA66 and actin (loading control) in HeLa cells 48 h after transfection with H_2O (−siRNA) or *HCA66* siRNAs (+siRNA). (**B**) Neo-synthesized RNAs from HeLa cells transfected with *HCA66* siRNAs (lanes 7–12) or mock-transfected (lanes 1–6) were pulse labeled with L-methyl ^{3}H methionine 48-h post-transfection and cells were harvested after the indicated chase times. Total RNAs extracted from these cells were separated by electrophoresis, transferred to a nylon membrane and labeled RNAs were detected by autoradiography.

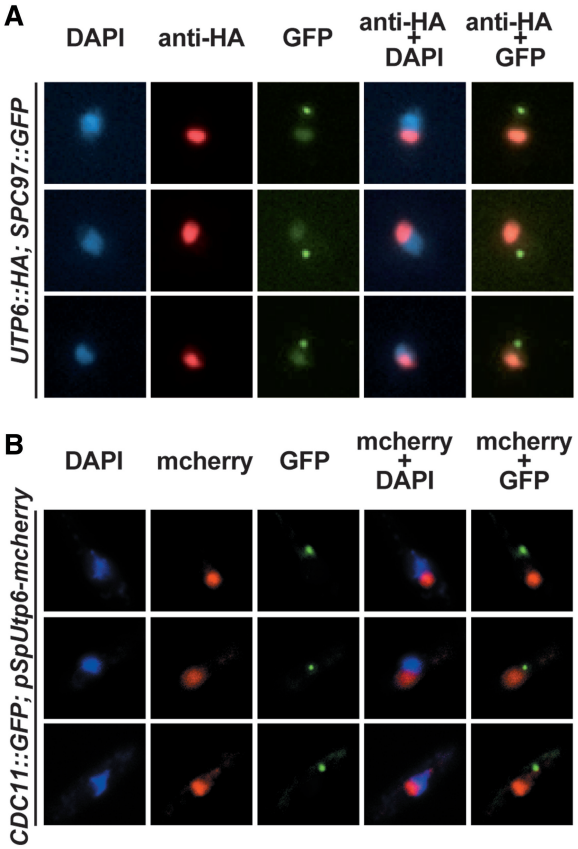

Figure 4. The homologues of HCA66 in *S. cerevisiae* and *S. pombe* cells are not detectable at the SPB. (**A**) Immunofluorescence microscopy using an *S. cerevisiae* strain expressing Utp6p-3HA (detected with anti-HA antibodies, red signal) and GFP-tagged Spc97p (green signal). (**B**) Fluorescence microscopy using an *S. pombe* strain expressing SpUtp6-mCherry (red signal) and Cdc11-GFP (green signal).

pre-ribosomes (41). HeLa cells were treated with siRNAs targeting *HCA66* mRNA and the localization of WDR36 or fibrillarin was assessed by immunofluorescence microscopy using specific antibodies (Supplementary Figure S1 and Supplementary Methods). HCA66 knockdown drastically affected the nucleolar localization of WDR36 and also that of fibrillarin to a lesser extent. Quantification of the nucleolar to nucleoplasmic signal ratios revealed a decrease by 64% for WDR36 and by 56% for fibrillarin. These data suggest that depletion of HCA66 affects early stages of ribosome synthesis and perturbs the nucleolar localization of other pre-rRNA processing factors.

To unambiguously demonstrate a direct role of HCA66 in pre-rRNA maturation, we assessed whether HCA66 interacts physically with pre-rRNAs or other components of the pre-ribosomal particles using co-immunoprecipitation experiments. The yeast homologue of HCA66, Utp6p, is a component of early 90S pre-ribosomes. We show here that immunoprecipitation of a 3HA-tagged version of Utp6p from a yeast cell extract results in co-purification of the U3 snoRNA and early pre-rRNAs (Supplementary Figure S2 and Supplementary Methods). Despite several attempts, we failed to co-immunoprecipitate early pre-rRNA intermediates or the U3 snoRNA with EGFP- and FLAG-tagged versions of HCA66 expressed in HeLa cells (data not shown). We suspect that this problem stems from the difficulty to solubilize sufficient amounts of nucleolar material containing the early pre-ribosomal particles under salt and detergent conditions that preserve integrity of the particles. We also carried out sedimentation experiments on density gradients to determine whether HCA66 co-sediments with pre-ribosomal particles (Supplementary Figure S3 and Supplementary Methods). HCA66 concentrated in the top fractions of the gradient, suggesting that part of the protein is engaged in small complexes or accumulates as a free entity at steady state. Of course, it is also possible that HCA66-containing large complexes were partially disrupted during extract preparation. Nevertheless, HCA66 is also present, albeit at lower

concentrations, throughout the gradient and co-sediments with various pre-rRNAs, including the earliest precursors, suggesting that HCA66 could be a component of different pre-ribosomal particles.

The centrosomal function of HCA66 is likely not conserved in the unicellular eukaryotes *S. cerevisiae* and *S. pombe*

We next studied whether the dual function of HCA66 in ribosome synthesis and at the centrosome is specific to human cells or widespread in eukaryotes. As previously observed by others (40,41), the protein displaying the highest homology with HCA66 (17% identity, 30% similarity) in the budding yeast *S. cerevisiae* is Utp6p, a component of the SSU processome shown to be required for the production of mature 18S rRNA (42). The function of HCA66/Utp6p in the synthesis of the small ribosomal subunit is therefore conserved in human and yeast cells. We first investigated whether, like HCA66, Utp6p also accumulates at the Spindle Pole Body (SPB), the functional equivalent of the centrosome in yeast cells. To compare the sub-cellular localization of Utp6p to that of a bona fide component of the SPB, we expressed a 3HA-tagged version of Utp6p in a strain expressing GFP-tagged Spc97p, a protein component of the yeast gamma-tubulin small complex (56) (Figure 4A). Addition of the 3HA tag to the C-terminus of Utp6p does not modify the growth rate of strain *SPC97::GFP* (data not shown), suggesting that it does not affect the function of Utp6p. Consistent with previous observations (42), the immunofluorescent signal corresponding to Utp6p-3HA stained the nucleolus, but it was not visible at the SPB, the dot-like structure containing Spc97p-GFP, even after long exposure times. To confirm these observations and exclude potential detection problems due to the immunostaining procedure, we fused the mCherry fluorescent protein to the C-terminus of Utp6p in strain *SPC97::GFP* and performed fluorescence microscopy (Supplementary Figure S4). The resulting images confirmed the absence of co-localization of Utp6p-mCherry and Spc97p-GFP at the SPB. They showed in addition that Utp6p-mCherry is not detected at the MTOCs in small budded cells displaying duplicated SPBs or in cells undergoing mitosis, suggesting that, unlike human HCA66 protein, yeast Utp6p does not accumulate at the MTOC during S phase and mitosis.

In human cells, γ-tubulin is a major component of the pericentriolar material and it is found in two main complexes: the γ-tubulin Small Complex (γ-TuSC), also containing the GCP2 and GCP3 proteins, and the γ-tubulin Ring Complex (γ-TuRC) resulting from the association between several γ-TuSCs and additional proteins such as GCP4, GCP5 and GCP6 (57). Interestingly, proteins homologous to GCP4, GCP5 and GCP6 are expressed in the fission yeast *S. pombe* (Gfh1, Mod21 and Alp16, respectively) but not in *S. cerevisiae*. Because the composition of the SPB in *S. pombe* shares more components with the human centrosome as compared to the budding yeast SPB, we next undertook a localization study of the homologue of HCA66 in fission yeast. The uncharacterized *SPBC244.02c S. pombe* gene encodes a protein (referred to as SpUtp6 afterward) displaying the highest homology with HCA66 (18% identity and 34% similarity). We constructed a vector in which the *SPBC244.02c* open reading frame (ORF) is fused to a sequence encoding the mCherry fluorescent moiety and placed under the control of the thiamine-repressible promoter. This construct was transformed into a *S. pombe* strain expressing GFP-tagged Cdc11, a SPB marker (46,47). Fluorescence microscopy revealed that the homologue of HCA66 in *S. pombe* cells accumulates exclusively in the nucleolus and is not detectable at the SPB containing Cdc11-GFP (Figure 4B). In conclusion, our results suggest that in the unicellular eukaryotes *S. cerevisiae* and *S. pombe*, the homologues of HCA66 do not accumulate at the MTOC. We cannot formally exclude however that the proteins are present in these structures at levels below the detection limits of our approaches.

To further investigate whether Utp6p functions only in ribosome synthesis in budding yeast or is also required for proper progression through mitosis, we compared the consequences of Utp6p or Spc97p depletion on cell cycle progression and ribosome synthesis. In yeast, the inactivation of factors required for ribosome biogenesis has been shown to delay the G1/S transition of the cell cycle and to result in the accumulation of G1 phase cells (6). In contrast, although SPB duplication occurs during the G1 phase of the cell cycle, defects in this process are not detected until mitosis, when cells need to set up a bipolar mitotic spindle in order to segregate DNA (58,59). Such defects result in the formation of aberrant monopolar mitotic spindles, which activate the spindle assembly checkpoint and induce a transient cell cycle arrest in mitosis. Yeast strains conditionally expressing 3HA-tagged versions of Utp6p or Spc97p from the *GAL1* promoter were shifted from galactose- to glucose-containing medium to deplete the corresponding proteins. Cell samples were harvested before and at different times after the shift and processed for western-blot analyses to assess depletion of the 3HA-tagged proteins (Figure 5A) or for fluorescence-activated cell sorting (FACS) to analyze the proportion of cells in the different phases of the cell cycle (Figure 5B). Consistent with the function of Spc97p at the SPB, FACS analyses revealed that cells undergoing Spc97p depletion accumulated in the G2/M phase of the cell cycle. This increase in G2/M cells is already visible in the *GAL::3HA::SPC97* strain grown on galactose-containing medium as compared to the wild-type strain, but this abnormal cell cycle profile does not translate into a detectable growth defect (data not shown). This observation indicates that the level of expression of 3HA-Spc97p in this strain and/or the N-terminal fusion to the tag affect to some extent the function of the fusion protein. The proportion of cells in G2/M phase rapidly increased over the depletion time course while the G1 peak disappeared. From 4 h and afterward, we observed an increase in the amount of cells with aberrant DNA contents and the appearance of a sub-G1 peak associated with cell death. In sharp contrast to the depletion of Spc97p, cells undergoing transcriptional

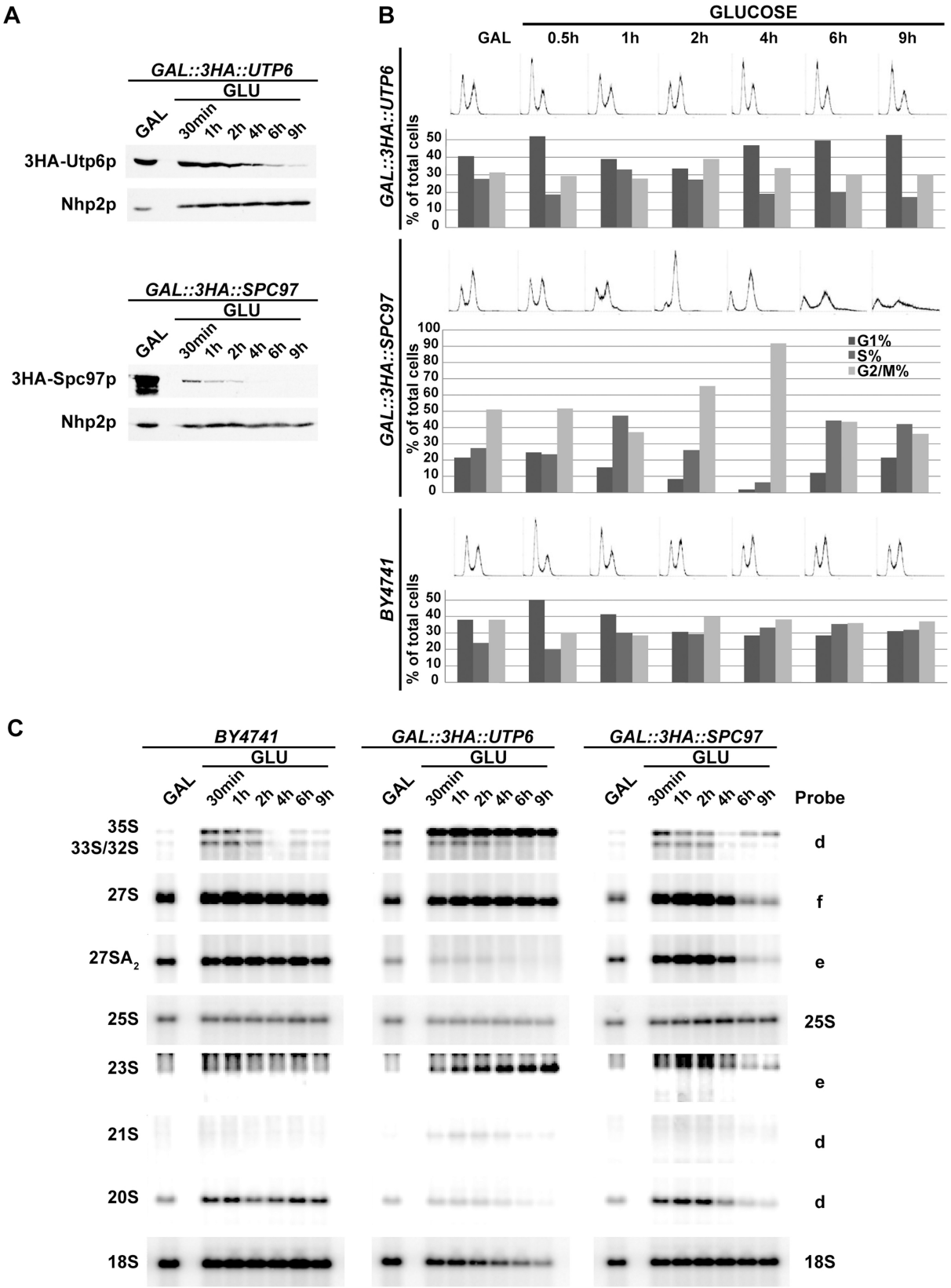

Figure 5. Depletion of Utp6p does not arrest cells in mitosis but induces pre-rRNA processing defects that delay G1 phase progression. (**A**) Western-blot analysis showing the depletion of 3HA-Utp6p and 3HA-Spc97p in strains *GAL::3HA::UTP6* and *GAL::3HA::SPC97*, respectively, shifted from a galactose- (GAL) to a glucose-based medium (GLU). (**B**) FACS analysis of cells undergoing 3HA-Utp6p or 3HA-Spc97p depletion, or wild-type cells (BY4741) as a control, showing the distribution of cells in the different cell cycle stages (G1, S and G2/M). (**C**) Northern-blot analysis of the pre-rRNA processing pathway in wild-type cells (BY4741) or cells undergoing 3HA-Utp6p or 3HA-Spc97p depletion using the indicated oligonucleotide probes (Supplementary Table S1).

repression of *UTP6* displayed a cell cycle profile that remained fully comparable to that of the WT cells up to 4 h following the nutritional shift. From 4 h and afterward, the *GAL::3HA::UTP6* strain displayed a significant accumulation of cells in G1 while the G2/M peak decreased as compared to control cells. Therefore, the cell cycle profiles observed in cells undergoing Utp6p depletion are clearly distinct from those observed in cells deprived of Spc97p and are not consistent with a direct function of Utp6p in SPB duplication and chromosome segregation. We cannot formally exclude, however, that the G1 cell cycle delay observed in Utp6p-depleted cells precedes and masks a G2/M arrest potentially resulting from altered SPB function. To determine whether Utp6p depletion affects tubulin distribution in yeast cells, we carried out immunofluorescence microscopy using anti-α-tubulin antibodies in strain *GAL::3HA::UTP6* grown for 4 h on glucose-containing medium. As a control, strain *GAL::3HA::SPC97* was treated identically. As shown in Supplementary Figure S5, the vast majority of the cells lacking Spc97p accumulated as large budded cells with the DAPI-stained DNA located at the bud neck or partially segregated. Alpha-tubulin in these cells appeared either distributed throughout the cells as a granular signal or formed spindles that looked to be aberrantly positioned. Importantly, no such aberrant mitotic figures could be observed in *GAL::3HA::UTP6* cells grown on glucose. These cells appear much smaller, probably as a consequence of early G1 arrests, and most of them exhibit one or two foci of α-tubulin localized at the vicinity of the DAPI-stained DNA.

Since Utp6p is required for ribosome synthesis in yeast and because we suspected that depletion of factors required for SPB duplication and chromosome segregation such as Spc97p could affect ribosome biogenesis, we analyzed by Northern blot the pre-rRNA processing pathway in cells depleted of Utp6p or Spc97p (Figure 5C). The *GAL::3HA::UTP6* strain grown on galactose-containing medium displays significant pre-rRNA processing defects compared to the wild-type BY4741 strain, suggesting that overexpression of Utp6p and/or its fusion to the 3HA tag affect to some extent the function of the protein. Consistent with published results (41), these defects are characterized by the accumulation of the 35S pre-rRNA and depletion of the 33S/32S, $27SA_2$ and 20S intermediates resulting from early cleavages of the 35S transcript at sites A_0, A_1 and A_2. Transcriptional repression of *UTP6* induces a rapid worsening of these processing defects, as early as 30 min following the nutritional shift, and leads to a rapid depletion of the mature 18S rRNA. These defects in ribosome synthesis probably inhibit cell growth during the G1 phase of the cell cycle, delay the G1/S transition and result in the accumulation of cells in G1 as observed in Figure 5B. In contrast, depletion of Spc97p did not immediately affect ribosome synthesis since the pre-rRNA maturation pathway remained comparable to that of wild-type cells up to 4 h following the nutritional shift. Since the transient G2/M cell cycle arrest was detectable as early as 30 min after transfer of the *GAL::3HA::SPC97* strain to the glucose-containing medium, these results suggest that activation of the spindle assembly checkpoint does not immediately inhibit ribosome biogenesis. However, from 4 h following the nutritional shift, the *GAL::3HA::SPC97* strain displayed significant defects in ribosome biogenesis, characterized by a faint accumulation of the 35S pre-rRNA and a depletion of all tested pre-rRNAs. These data suggest that ribosome biogenesis is ultimately inhibited and the pre-ribosomal particles partially degraded in the aberrant cells undergoing Spc97p depletion.

Altogether, these results show that Utp6p depletion in yeast cells induces rapid defects in early steps of ribosome synthesis and results in the accumulation of cells in the G1 phase of the cell cycle. However, Utp6p is not detectable at the SPB and its depletion does not induce mitotic arrest, suggesting that Utp6p is not directly required for mitosis.

Some molecular mechanisms underlying the function of HCA66/Utp6p in ribosome synthesis are conserved in yeast and mammals

Utp6p contains three 'half a tetratricopeptide' (HAT) repeats (60,61) proposed to define a protein–protein interaction platform mediating the interaction with Utp21p, another component of the UTP-B module of the SSU processome (41). Substitution of a single amino acid, alanine 99, within the first HAT repeat of Utp6p affects pre-rRNA processing in yeast cells. This modification does not seem to prevent the incorporation of Utp6p into early pre-ribosomal particles, but disrupts the interaction between Utp6p and Utp21p *in vitro* and *in vivo* in a yeast two hybrid system (41). In addition, substitutions of other residues of the HAT repeats that are conserved among Utp6p orthologs (K102, D106, H140, E156 and R173), induce cryosensitive phenotypes suggesting that these residues are important for Utp6p function (60). HCA66 contains seven HAT repeats and consistent with previous observations (40), sequence comparison showed that the N-terminal region and the first three HAT repeats of HCA66 display the highest homology to Utp6p (Supplementary Figure S6), suggesting that this part of the protein is important for ribosome synthesis in human cells. We next undertook a mutational analysis in HeLa cells to determine to what extent the molecular function of HCA66 in ribosome synthesis is similar to that of Utp6p in yeast. We constructed vectors allowing expression of several modified versions of EGFP-tagged HCA66 featuring, within the first 3 HAT repeats of the protein, substitutions of specific amino acids homologous to the aforementioned residues of Utp6p important for function in ribosome synthesis (Figure 6A). We transfected these vectors into HeLa cells and showed that the corresponding modified proteins accumulated at similar levels as the wild-type protein (Supplementary Figure S7A and Supplementary Methods) and localized to the nucleoli (Supplementary Figure S7B and Supplementary Methods). To assess the functionality of these modified versions of HCA66 in ribosome synthesis, the constructs were transfected into HeLa cells together with siRNAs targeting the 3′-UTR of the endogenous *HCA66* mRNA. Such siRNAs are not complementary to the transcripts

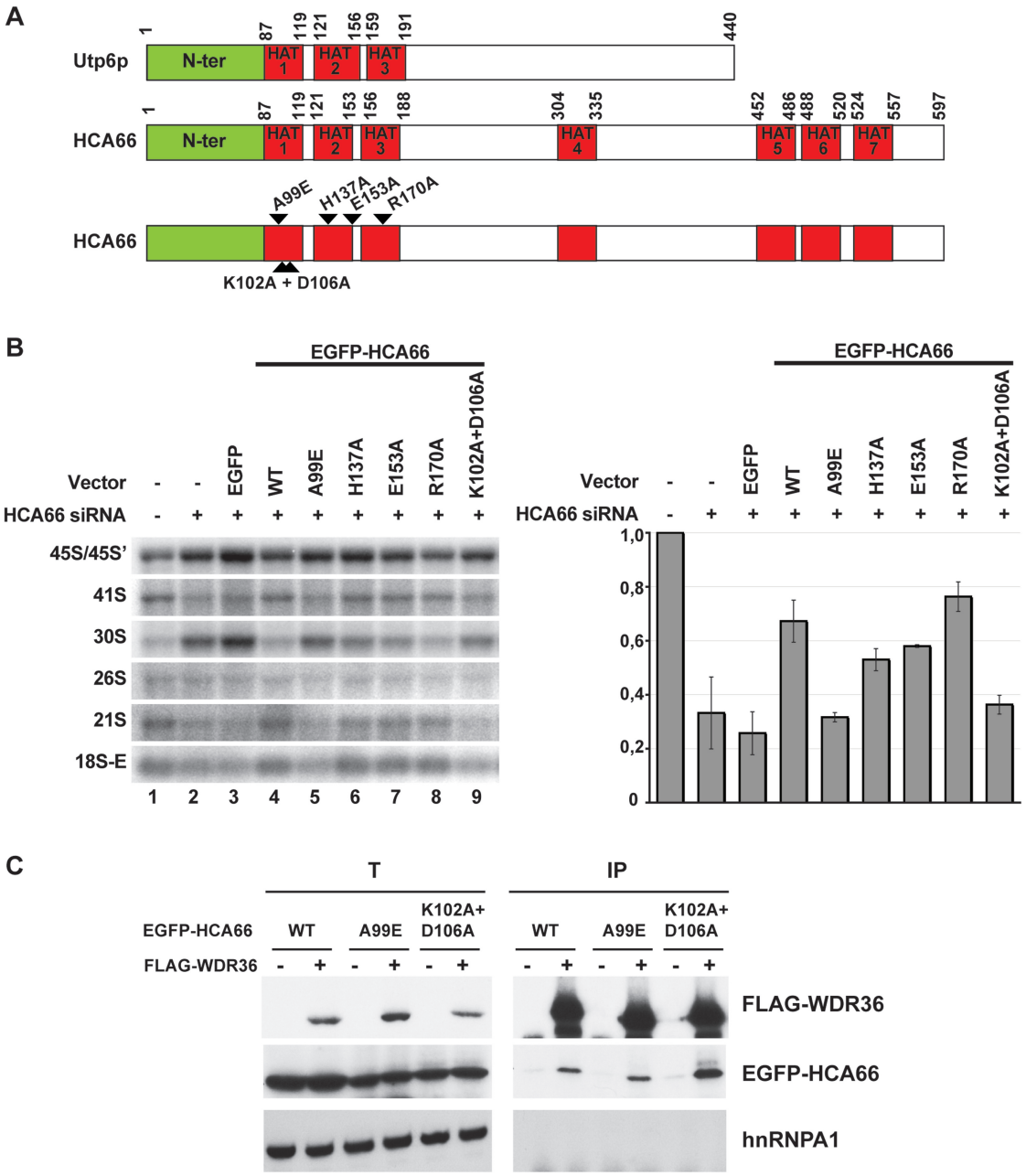

Figure 6. Some molecular mechanisms underlying the function of HCA66/Utp6p in ribosome synthesis are conserved in yeast and mammals. (**A**) Schematic representation of Utp6p (440 amino acids), HCA66 (597 amino acids) and the different modified versions of HCA66 bearing single (A99E, H137A, E153A, R170A) or double (K102A + D106A) amino acid substitutions within the HAT repeats. The conserved N-terminal domain is colored in green, the HAT motifs in red. (**B**) Northern-blot analysis showing the accumulation levels of some pre-rRNAs (indicated on the left) in HeLa cells transfected with siRNAs targeting the 3′-UTR of *HCA66* mRNA, either alone or in combination with vectors expressing EGFP only or wild-type and modified versions of EGFP-HCA66. The 18S-E/30S ratios, averaged from three experiments, are reported on the histogram presented on the right. (**C**) Immunoprecipitation experiment using anti-FLAG antibodies and HeLa cells co-expressing FLAG-WDR36 (+) or FLAG alone (−) and wild-type (WT) or altered version (A99E or K102A + D106A) of EGFP-HCA66. A fraction of the total extracts used for the experiments (T) and of the immunoprecipitated material (IP) was analyzed by western blot.

encoding the EGFP-tagged versions of HCA66 (bearing a different 3′-UTR) and therefore do not affect their stability. After 48 h of treatment, HeLa cells were harvested and we determined by Northern blot whether the altered versions of HCA66 rescue the pre-rRNA processing defects (quantified by calculating the 18S-E/30S ratio from PhosphorImager data) resulting from depletion of the endogenous protein (Figure 6B). Cells transfected with siRNAs alone (lane 2) or co-transfected with siRNAs and the vector encoding EGFP only (lane 3) displayed a strong decrease in the 18S-E/30S ratio (by ~70%) in comparison with control cells (lane 1). In contrast, co-transfection of the vector encoding EGFP-tagged wild-type HCA66 along with the siRNAs

(lane 4), tended to restore an 18S-E/30S ratio comparable to that observed in control cells, indicating that EGFP-HCA66 is functional and validating our experimental approach. Interestingly, expression of the EGFP-HCA66$_{A99E}$ protein (lane 5) did not compensate for the absence of the endogenous protein nor did the expression of a modified version of HCA66 featuring alanines instead of lysine 102 and aspartic acid 106 (lane 9). We concluded that these residues within the first HAT repeat of HCA66 are crucial for the function of the protein in ribosome synthesis, similarly to the results obtained with Utp6p in yeast (41,60). Expression of altered HCA66 proteins bearing amino acid substitutions within the second (H137A, lane 6) and third (E153A, lane 7) HAT motifs of HCA66 only partially alleviated the processing defects induced by the siRNA treatment, suggesting that these modifications affect to some extent the function of HCA66. Substitution of arginine 170 within the third HAT domain (lane 8) did not affect the function of the protein in the processing of the pre-rRNAs. These data show that some residues of the HAT repeats of Utp6p important for pre-rRNA processing in yeast are also required for the function of human HCA66, indicating that some molecular mechanisms underlying the function of the protein in ribosome synthesis are evolutionarily conserved.

Since the interaction of yeast Utp6p and Utp21p has been suggested to be important for pre-rRNA processing (41), we tested whether, similarly to Utp6p, HCA66 also displays functional connections with the human homologue of yeast Utp21p, WDR36. We co-expressed in HeLa cells wild-type EGFP-HCA66 or the EGFP-HCA66$_{A99E}$ and EGFP-HCA66$_{K102A/D106A}$ altered proteins with either a FLAG-tagged version of WDR36 or the FLAG moiety alone, and we carried out immunoprecipitation experiments using a chromatography matrix conjugated with anti-FLAG antibodies (Figure 6C). EGFP-HCA66 was detected significantly above background levels in the FLAG-WDR36 immunoprecipitate suggesting that the two proteins interact physically in HeLa cells. This interaction is specific since it was not observed when FLAG alone was transfected along with EGFP-HCA66, and since the abundant nuclear protein hnRNP A1 is not co-immunoprecipitated with FLAG-WDR36 in the same conditions. Northern-blot analyses showed that early pre-ribosomal RNAs such as the 45S/45S′, 43S and 41S intermediates are not present in the extracts prepared for the co-immunoprecipitation experiments (data not shown), suggesting that early pre-ribosomes were either not solubilized or partially disrupted during extract preparation. The observed interaction between EGFP-HCA66 and FLAG-WDR36 may therefore result from direct contacts between the two proteins or occur within small modules such as the equivalent of the yeast UTP-B module. Surprisingly, the EGFP-HCA66$_{A99E}$ protein was found to interact with FLAG-WDR36 as efficiently as the wild-type protein (Figure 6C), although this amino acid substitution has been shown to disrupt the interaction between the homologous yeast proteins *in vitro* and in a yeast two hybrid system (41). The EGFP-HCA66$_{K102A/D106A}$ protein also interacts with FLAG-WDR36. Both altered proteins accumulate in the nucleoli of HeLa cells (Supplementary Figure S7B), suggesting that they are efficiently incorporated into pre-ribosomal particles. In addition to the Utp6p-Utp21p interaction, many other protein–protein contacts have been proposed to connect the different components of the UTP-B module (41) and these additional contacts may strengthen the interaction between EGFP-HCA66$_{A99E}$ and FLAG-WDR36 *in vivo*. Alternatively, the direct interaction between yeast Utp6p and Utp21p proteins may not be conserved in human cells or involve different amino acids.

Centrosome duplication and ribosome synthesis are not intimately connected in HeLa cells

The functions of HCA66 in ribosome synthesis and centrosome duplication may allow a connection between these two processes or alternatively, they may be independent. Our experiments presented in Figure 5 showed that depletion of the SPB component Spc97p in yeast cells does not affect initially ribosome synthesis, suggesting that interference with some aspects of SPB maturation or function does not result in direct defects in ribosome synthesis. We next investigated whether the functions of HCA66 in centrosome duplication and ribosome synthesis are coupled or independent and whether some aspects of these two processes are interconnected in HeLa cells. We took advantage of a previously described truncated form of HCA66, corresponding to the first 86 amino acids of the protein. When overexpressed in U2OS cells, the EGFP-HCA66$_{1–86}$ fusion protein accumulates only at the centrosome and affects centrosome function in a dominant negative manner (40). We expressed EGFP-HCA66$_{1–86}$ in HeLa cells to perturb centrosome function and assessed the consequences on ribosome biogenesis. The cell cycle profile of HeLa cells expressing EGFP-HCA66$_{1–86}$ 48-h post-transfection displayed a prominent 'sub-G1' peak, corresponding to cells containing less than one DNA content (Figure 7A). In addition, we noticed that cultures of cells expressing EGFP-HCA66$_{1–86}$ contained a higher proportion of trypan blue-positive cells, indicative of increased cell death (Figure 7B). This phenotype seems to result at least in part from apoptosis as suggested by the presence of fragmented genomic DNA in cells expressing EGFP-HCA66$_{1–86}$ as compared to control cells (Figure 7C). These data suggest that perturbing HCA66 function at the centrosome through over-expression of EGFP-HCA66$_{1–86}$ in HeLa cells results in cell death by apoptosis. To analyze the consequences of these defects on pre-rRNA processing, equal amounts of RNAs extracted from HeLa cells expressing EGFP, EGFP-HCA66, EGFP-HCA66$_{1–86}$ or mock-transfected cells were analyzed by Northern blotting (Figure 7D). The pre-rRNA processing profile in cells expressing EGFP-HCA66$_{1–86}$ was qualitatively fully comparable to that observed in control cells even 72 h after electroporation. In particular, the pre-rRNA processing defects characteristic of impaired HCA66 function were not observed, indicating that altering specifically the function of HCA66 at the centrosome has no impact on

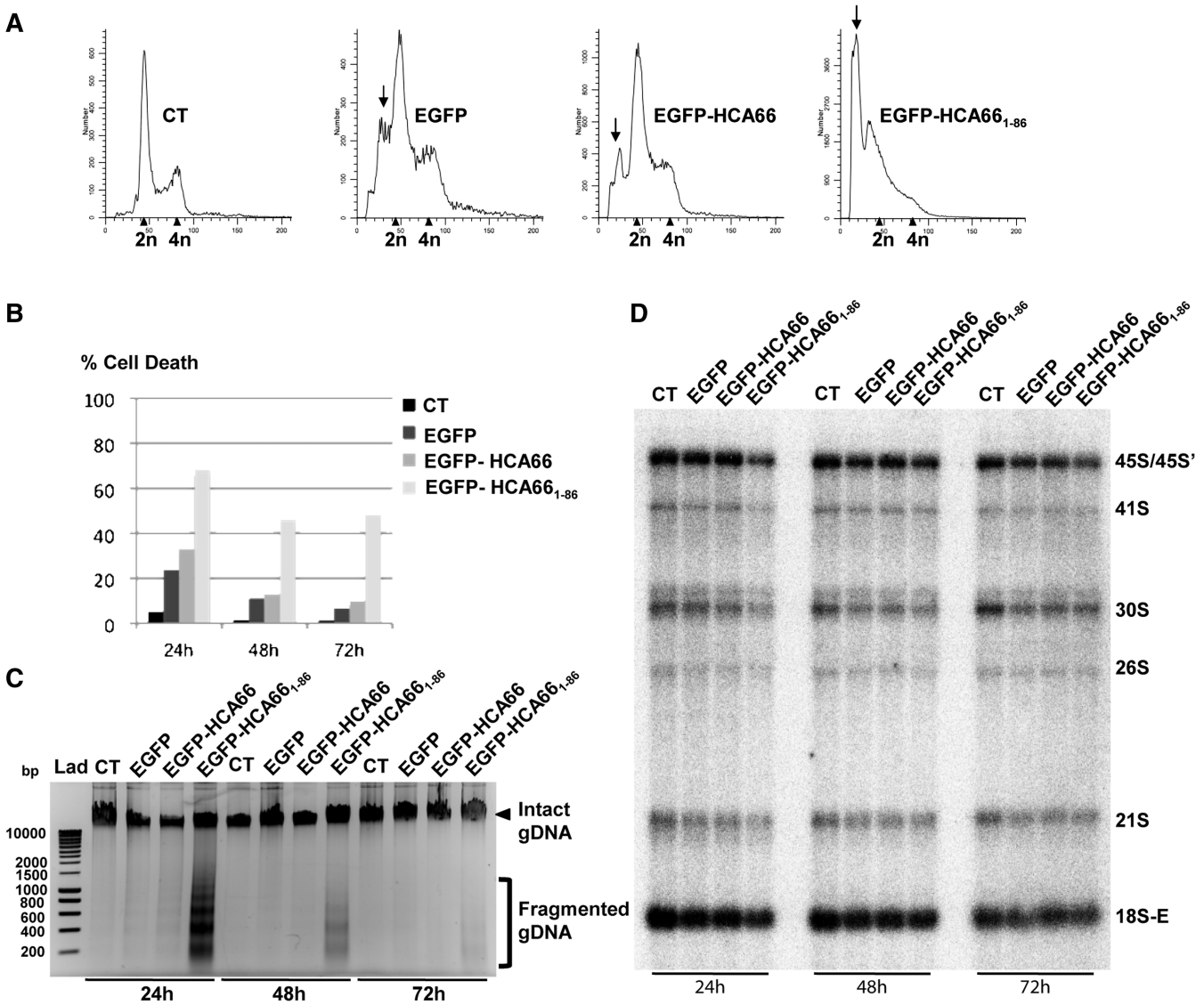

Figure 7. Defects in centrosome function induced by the expression of a dominant negative version of HCA66 do not impair ribosome synthesis in HeLa cells. (**A**) FACS analysis showing the cell cycle profiles of HeLa cell cultures expressing EGFP, EGFP-HCA66, EGFP-HCA66$_{1–86}$ or mock-transfected 48 h after transfection. Total cells (adherent and floating cells) were analyzed in each case. The arrowheads below each graph indicate the positions of the G1 and G2/M peaks. Arrows indicate the presence of a sub-G1 peak, prominent in cells expressing EGFP-HCA66$_{1–86}$. (**B**) Proportion of dead cells in cultures expressing EGFP, EGFP-HCA66, EGFP-HCA66$_{1–86}$ or mock-transfected 24, 48 or 72 h after electroporation. The histogram represents the percentage of trypan blue positive (dead) cells in each population, considering total cells. (**C**) Agarose gel electrophoresis of genomic DNAs extracted from HeLa cells expressing EGFP, EGFP-HCA66, EGFP-HCA66$_{1–86}$ or mock-transfected, 24, 48 or 72 h after electroporation. Genomic DNAs have been extracted from total cells. Molecular weight ladder: SmartLadder (Eurogentec). (**D**) Northern-blot analysis using probe a (Figure 2B and Supplementary Table S1) showing the accumulation levels of some pre-rRNAs in HeLa cells expressing EGFP, EGFP-HCA66, EGFP-HCA66$_{1–86}$ or mock-transfected, 24, 48 or 72 h after electroporation. RNAs were extracted from total cells.

the nucleolar function of the protein. The slight global decrease in the accumulation levels of all pre-rRNA intermediates observed 24 h after electroporation is likely due to the high number of dead cells at this time point (nearly 70%). Indeed, Northen-blot analysis of total RNAs corresponding to equal amounts of adherent cells confirmed a global reduction of all tested precursor and mature rRNAs (and very likely also of all other cellular RNAs) in cells expressing EGFP-HCA66$_{1–86}$, probably due to global degradation of cellular RNAs in the pre-apoptotic cells (Supplementary Figure S8).

We next affected centrosome function by interfering with the expression of NEDD1, another essential component of the peri-centriolar material in human cells (51). We treated HeLa cells with siRNAs targeting *NEDD1* mRNA or scrambled siRNAs as a control, and we analyzed the consequences on pre-rRNA processing 48 h after transfection by Northern blot (Supplementary Figure S9). Although the NEDD1 protein was significantly depleted, no defect in the maturation of the pre-rRNAs was observed in contrast to what was observed in cells treated with *HCA66* siRNAs.

We concluded from these observations that at least some aspects of centrosome duplication and ribosome synthesis are not intimately connected in HeLa cells. Altering the centrosomal function of HCA66 through the over-expression of a dominant negative version of the protein does not impair its nucleolar function, suggesting that these two functions are independent.

DISCUSSION

HCA66 was initially characterized as a component of the centrosome and was shown to be required for centriole duplication and the establishment of a bipolar spindle ensuring proper chromosome segregation during mitosis (40). In addition, HCA66 accumulates prominently in the nucleoli and our results showed that this localization probably reflects a function in ribosome biogenesis. RNAi-mediated depletion of HCA66 in human cells impairs removal of the 5′ETS of the pre-ribosomal RNAs and the production of the mature 18S rRNA, indicating that HCA66 is required for the synthesis of the 40S ribosomal subunit. Partial depletion of HCA66 also interferes with the nucleolar accumulation of WDR36 and fibrillarin. In mammalian cells, HCA66 is therefore required for both centriole duplication and ribosome biogenesis. Interestingly, B23/nucleophosmin (NPM) is another factor accumulating both at the centrosome and in the nucleoli that was shown to be involved in both centriole duplication and ribosome synthesis in mammalian cells. In the nucleoli, B23/NPM has been suggested to function as an endoribonuclease in the processing of the pre-rRNA within ITS2 and to be required for the synthesis of the large ribosomal subunit (62). The cell cycle-dependent centrosome association of B23/NPM is somewhat different from that of HCA66 since HCA66 is detected at the centrosome from the beginning of S phase, when centrosome duplication occurs, to the end of mitosis (40), whereas B23/NPM seems to dissociate from the centrosome during G1 phase and to re-associate with the mitotic poles during mitosis (37). The dissociation of B23/NPM from the centrosome during the G1 phase is required for centriole duplication (37). Therefore, while HCA66 is required for centriole duplication, B23/NPM seems to have an antagonistic function on this process. It has been proposed that B23/NPM provides a licensing system allowing the coordination of centrosome duplication with DNA replication at the beginning of S phase (37).

The function of HCA66 in ribosome synthesis is conserved in eukaryotes, since Utp6p in yeast is also a component of early pre-ribosomal particles and is required for early pre-rRNA cleavages and 40S ribosomal subunit production (41,42). A truncated version of Utp6p encompassing the N-terminal domain and the 3 HAT repeats of the protein is sufficient to support ribosome biogenesis and cell viability under physiological conditions, indicating that this minimal protein retains all the biochemical properties relevant to the function in ribosome synthesis (41). The N-terminal and HAT domains of Utp6p have been suggested to mediate physical interactions with Utp18p and Utp21p, respectively, two other components of the UTP-B module of the 90S pre-ribosomal particle (41). The G99A substitution in the first HAT repeat of Utp6p disrupts the interaction with Utp21p but does not prevent the incorporation of the modified protein into pre-ribosomes (41). Interestingly, we showed that several amino acid substitutions within the first HAT repeat of HCA66, in particular the A99E substitution, are deleterious for pre-rRNA processing, indicating that these residues are important for the nucleolar function of HCA66. Nevertheless, the $HCA66_{A99E}$ altered protein accumulated in the nucleoli and was found associated with WDR36, probably within small modules deriving from, or in their way to be incorporated into, the early pre-ribosomal particles. Altogether, these results show that at least some aspects of the precise molecular function of Utp6p/HCA66 in ribosome synthesis are conserved in yeast and mammals. However, expression of HCA66 in yeast cells lacking Utp6p does not restore cell viability and HCA66 is not incorporated into yeast pre-ribosomes, as assessed by immunoprecipitation experiments (A.K.H., unpublished data). As mentioned in the introduction, it was proposed that defects in early steps of ribosome synthesis in yeast cells delay the G1/S transition before they result in a depletion of mature ribosomes and a global defect in protein synthesis (6). In our experiments presented in Figure 5, the *GAL::3HA::UTP6* strain displays significant pre-rRNA processing defects when grown on galactose and early after transfer to the glucose-containing medium but unexpectedly, the cell cycle profiles in these conditions remain very similar to the ones observed in wild-type cells. Accumulation of G1 phase cells is visible only 4 h after transfer to glucose-containing medium and seems to correlate better with a significant depletion of the mature 18S rRNA and most likely with an imbalance in ribosomal subunits. This apparent contradiction with previous results may stem from the difference of the strains analyzed (a *GAL::3HA::PWP2* strain was used by Bernstein and co-workers) and the time needed to deplete the corresponding proteins. In addition, the G1/S transition delays reported by Bernstein and co-workers were inferred from the increase in the proportion of unbudded cells, a technique with a different sensitivity as compared to FACS.

The function of HCA66 in centriole duplication does not seem to be conserved in unicellular eukaryotes. Utp6p is not detectable at the SPB in *S. cerevisiae* cells, neither is the homologous protein in *S. pombe*. In addition, transcriptional repression of *UTP6* in budding yeast does not result in a G2/M cell cycle arrest as observed in cells undergoing depletion of bona fide components of the SPB. Given that the function of the protein in ribosome synthesis is conserved from yeast to mammals, it is tempting to speculate that its MTOC-related function appeared during evolution as a gain of function in an ancestral factor involved in ribosome synthesis. Since the HAT repeats of Utp6p have been suggested to mediate protein–protein interactions, this biochemical property of the protein may have been mobilized during evolution to fulfill other functions in addition to the assembly of the

pre-ribosomal particle. Alternatively, we cannot exclude that HCA66 derives from an ancestral protein displaying a dual function in ribosome synthesis and MTOC duplication, and that this latter function has been lost during evolution in some unicellular eukaryotes. Consistently, gamma-tubulin complexes in budding yeast assemble in a small form, from the three proteins gamma-tubulin, Spc97p, and Spc98p, whereas the assembly and spindle recruitment of gamma-tubulin complexes in most other eukaryotes involves a multitude of accessory proteins. HCA66 in humans may therefore exert a function in regulating gamma-tubulin complex components by interacting with one of these accessory proteins (40). It would be interesting to study the functions of the homologues of HCA66 in various other eukaryotic organisms to determine whether it has a conserved role at the centrosome and in gamma-tubulin regulation.

Several hypotheses can be considered concerning the biological significance of the dual function of HCA66 in HeLa cells. The protein could be recruited separately at the centrosome and in the nucleoli and it could function independently in these two structures. Alternatively, the centrosomal and nucleolar functions of HCA66 could be interconnected and may allow some sort of coordination between the two processes. For example, the protein may need to function in one process, and transit either through the nucleolus or through the centrosome, to undergo some modifications and/or to interact with some RNA or protein partners in order to acquire its functionality for the other process. Based on the fact that the accumulation of HCA66 at the centrosome and in the nucleoli is dynamic depending on the stages of the cell cycle (40), another view could be that HCA66 is sequestered or fully mobilized in one structure at a specific stage of the cell cycle and needs to be released to fulfill the second function at other stages. For example, HCA66 accumulates in the nucleoli, but not at the centrosome in G1 phase, and a fraction of the protein could be released from the nucleoli following the G1/S transition to function at the centrosome. To start addressing the biological significance of the dual function of HCA66, we interfered specifically with the function of the protein at the centrosome through the expression $HCA66_{1–86}$ and we assessed the consequences on the nucleolar function. When expressed in U2OS cells, EGFP-$HCA66_{1–86}$ accumulates exclusively at the centrosome and perturbs its function (40). Our results show that in HeLa cells, expression of this truncated protein, which also appears restricted to the centrosome (C.B., unpublished data), results in apoptosis. This result could be consistent with previous observations that HCA66 interacts with Apaf-1, a component of the apoptosome (39). Overexpression of full length HCA66 potentiates Apaf-1-dependent apoptosis, whereas overexpression of a truncated version of HCA66 consisting of the first 207 amino acids of the protein interferes with this process (39). This N-terminal domain of HCA66 is sufficient to mediate the interaction with Apaf-1, but a shorter fragment consisting of the first 190 residues does not interact with Apaf-1 *in vivo* and its overexpression has no effect on Apaf-1-dependent apoptosis. According to these results, the $HCA66_{1–86}$ construct is not expected to interact with Apaf-1 and therefore, its overexpression may not influence the Apaf-1-dependent pathway. Surprisingly, the pre-rRNA maturation profile in cells expressing $HCA66_{1–86}$ remains unaffected, suggesting that altering specifically the function of HCA66 at the centrosome does not impair its function in ribosome biogenesis. More generally, our results suggest that some defects in centrosome duplication do not have a major impact on ribosome synthesis and therefore, at least some aspects of these two essential cellular processes are not intimately connected in HeLa cells. Interestingly, the same conclusion can be drawn from our results obtained in yeast cells. Depletion of the SPB protein Spc97p in yeast cells induces a rapid cell cycle arrest in the G2/M phase, most likely reflecting the activation of the spindle assembly checkpoint. Our Northern-blot data show that when this cell cycle arrest occurs, synthesis and maturation of the 35S pre-rRNA proceed unabated. Therefore, defects in SPB duplication and activation of the spindle assembly checkpoint in yeast cells do not directly impair ribosome synthesis. However, long-term depletion of SPB components ultimately results in the appearance of aberrant cells in which significant defects in ribosome synthesis are observed. We conclude that both in yeast and HeLa cells, there is no obvious communication between centrosome function and ribosome synthesis.

SUPPLEMENTARY DATA

Supplementary Data are available at NAR Online: Supplementary Table 1, Supplementary Figures 1–9, Supplementary Methods and Supplementary Reference [63].

ACKNOWLEDGEMENTS

We are highly indebted to Andreas Merdes and Laurence Haren for reagents, technical help, helpful discussions and critical comments on the manuscript. We thank M. Faubladier, C. Caron, V. Cadamuro, M.-F. O'Donohue, P.-E. Gleizes, K. Bystricky, O. Gadal, C. Dez, M. Dalvai, O. Humbert, A. Timmers and all members of our group as well as Y. Gachet, S. Tournier (LBCMCP, Toulouse), P. Bouvet (ENS, Lyon), D. Zerbib (IPBS, Toulouse), A. Diot and P. Belenguer (CBD, Toulouse) for reagents, strains, technical help and helpful discussions. We also acknowledge A. Leru, M. Quaranta and the use of the FACS facility of CBD/IFR109.

FUNDING

Centre National de la Recherche Scientifique (CNRS), Université Paul Sabatier; Agence Nationale de la Recherche (ANR) (to Y.H.); Ligue Contre le Cancer ('Equipe labellisée') (to Y.H. and A.K.H.); Fondation pour la Recherche Médicale (to T.K.); Ligue Contre le Cancer (fellowships to M.G.); Fondation pour la Recherche Médicale (FRM) (fellowships to M.G.); Carrier Development Award from the Human Frontier

Science Program Organization (HFSPO) (to A.K.H.). Funding for open access charge: HFSPO.

Conflict of interest statement. None declared.

REFERENCES

1. Henras,A.K., Soudet,J., Gérus,M., Lebaron,S., Caizergues-Ferrer,M., Mougin,A. and Henry,Y. (2008) The post-transcriptional steps of eukaryotic ribosome biogenesis. *Cell. Mol. Life Sci.*, **65**, 2334–2359.
2. Kressler,D., Hurt,E. and Bassler,J. (2010) Driving ribosome assembly. *Biochim. Biophys. Acta*, **1803**, 673–683.
3. Panse,V.G. and Johnson,A.W. (2010) Maturation of eukaryotic ribosomes: acquisition of functionality. *Trends Biochem. Sci.*, **35**, 260–266.
4. Russell,J. and Zomerdijk,J.C. (2005) RNA-polymerase-I-directed rDNA transcription, life and works. *Trends Biochem. Sci.*, **30**, 87–96.
5. Clemente-Blanco,A., Mayán-Santos,M., Schneider,D.A., Machín,F., Jarmuz,A., Tschochner,H. and Aragon,L. (2009) Cdc14 inhibits transcription by RNA polymerase I during anaphase. *Nature*, **458**, 219–222.
6. Bernstein,K.A., Bleichert,F., Bean,J.M., Cross,F.R. and Baserga,S.J. (2007) Ribosome biogenesis is sensed at the Start cell cycle checkpoint. *Mol. Biol. Cell*, **18**, 953–964.
7. Rosado,I.V., Kressler,D. and de la Cruz,J. (2007) Functional analysis of Saccharomyces cerevisiae ribosomal protein Rpl3p in ribosome synthesis. *Nucleic Acids Res.*, **35**, 4203–4213.
8. Grimm,T., Hölzel,M., Rohrmoser,M., Harasim,T., Malamoussi,A., Gruber-Eber,A., Kremmer,E. and Eick,D. (2006) Dominant-negative Pes1 mutants inhibit ribosomal RNA processing and cell proliferation via incorporation into the PeBoW-complex. *Nucleic Acids Res.*, **34**, 3030–3043.
9. Hölzel,M., Rohrmoser,M., Schlee,M., Grimm,T., Harasim,T., Malamoussi,A., Gruber-Eber,A., Kremmer,E., Hiddemann,W., Bornkamm,G.W. *et al.* (2005) Mammalian WDR12 is a novel member of the Pes1-Bop1 complex and is required for ribosome biogenesis and cell proliferation. *J. Cell Biol.*, **170**, 367–378.
10. Iwanami,N., Higuchi,T., Sasano,Y., Fujiwara,T., Hoa,V.Q., Okada,M., Talukder,S.R., Kunimatsu,S., Li,J., Saito,F. *et al.* (2008) WDR55 is a nucleolar modulator of ribosomal RNA synthesis, cell cycle progression, and teleost organ development. *PLoS Genet.*, **4**, e1000171.
11. Lapik,Y.R., Fernandes,C.J., Lau,L.F. and Pestov,D.G. (2004) Physical and functional interaction between Pes1 and Bop1 in mammalian ribosome biogenesis. *Mol. Cell*, **15**, 17–29.
12. Pestov,D.G., Strezoska,Z. and Lau,L.F. (2001) Evidence of p53-dependent cross-talk between ribosome biogenesis and the cell cycle: effects of nucleolar protein Bop1 on G(1)/S transition. *Mol. Cell. Biol.*, **21**, 4246–4255.
13. Bhat,K.P., Itahana,K., Jin,A. and Zhang,Y. (2004) Essential role of ribosomal protein L11 in mediating growth inhibition-induced p53 activation. *EMBO J.*, **23**, 2402–2412.
14. Dai,M.S., Zeng,S.X., Jin,Y., Sun,X.X., David,L. and Lu,H. (2004) Ribosomal protein L23 activates p53 by inhibiting MDM2 function in response to ribosomal perturbation but not to translation inhibition. *Mol. Cell. Biol.*, **24**, 7654–7668.
15. Rubbi,C.P. and Milner,J. (2003) Disruption of the nucleolus mediates stabilization of p53 in response to DNA damage and other stresses. *EMBO J.*, **22**, 6068–6077.
16. Yuan,X., Zhou,Y., Casanova,E., Chai,M., Kiss,E., Gröne,H.J., Schütz,G. and Grummt,I. (2005) Genetic inactivation of the transcription factor TIF-IA leads to nucleolar disruption, cell cycle arrest, and p53-mediated apoptosis. *Mol. Cell*, **19**, 77–87.
17. Lindström,M.S. and Nistér,M. (2010) Silencing of ribosomal protein S9 elicits a multitude of cellular responses inhibiting the growth of cancer cells subsequent to p53 activation. *PLoS One*, **5**, e9578.
18. Lindström,M.S. and Zhang,Y. (2008) Ribosomal protein S9 is a novel B23/NPM-binding protein required for normal cell proliferation. *J. Biol. Chem.*, **283**, 15568–15576.
19. Llanos,S. and Serrano,M. (2010) Depletion of ribosomal protein L37 occurs in response to DNA damage and activates p53 through the L11/MDM2 pathway. *Cell Cycle*, **9**, 4005–4012.
20. Sun,X.X., Wang,Y.G., Xirodimas,D.P. and Dai,M.S. (2010) Perturbation of 60 S ribosomal biogenesis results in ribosomal protein L5- and L11-dependent p53 activation. *J. Biol. Chem.*, **285**, 25812–25821.
21. Castle,C.D., Cassimere,E.K., Lee,J. and Denicourt,C. (2010) Las1L is a nucleolar protein required for cell proliferation and ribosome biogenesis. *Mol. Cell. Biol.*, **30**, 4404–4414.
22. Dai,M.S., Sun,X.X. and Lu,H. (2008) Aberrant expression of nucleostemin activates p53 and induces cell cycle arrest via inhibition of MDM2. *Mol. Cell. Biol.*, **28**, 4365–4376.
23. Hölzel,M., Orban,M., Hochstatter,J., Rohrmoser,M., Harasim,T., Malamoussi,A., Kremmer,E., Längst,G. and Eick,D. (2010) Defects in 18 S or 28 S rRNA processing activate the p53 pathway. *J. Biol. Chem.*, **285**, 6364–6370.
24. Ma,H. and Pederson,T. (2007) Depletion of the nucleolar protein nucleostemin causes G1 cell cycle arrest via the p53 pathway. *Mol. Biol. Cell*, **18**, 2630–2635.
25. McMahon,M., Ayllón,V., Panov,K.I. and O'Connor,R. (2010) Ribosomal 18 S RNA processing by the IGF-I-responsive WDR3 protein is integrated with p53 function in cancer cell proliferation. *J. Biol. Chem.*, **285**, 18309–18318.
26. Peng,Q., Wu,J., Zhang,Y., Liu,Y., Kong,R., Hu,L., Du,X. and Ke,Y. (2010) 1A6/DRIM, a novel t-UTP, activates RNA polymerase I transcription and promotes cell proliferation. *PLoS One*, **5**, e14244.
27. Wang,Y., Liu,J., Zhao,H., Lü,W., Zhao,J., Yang,L., Li,N., Du,X. and Ke,Y. (2007) Human 1A6/DRIM, the homolog of yeast Utp20, functions in the 18S rRNA processing. *Biochim. Biophys. Acta*, **1773**, 863–868.
28. Yu,W., Qiu,Z., Gao,N., Wang,L., Cui,H., Qian,Y., Jiang,L., Luo,J., Yi,Z., Lu,H. *et al.* (2010) PAK1IP1, a ribosomal stress-induced nucleolar protein, regulates cell proliferation via the p53-MDM2 loop. *Nucleic Acids Res.*, **39**, 2234–2248.
29. Deisenroth,C. and Zhang,Y. (2010) Ribosome biogenesis surveillance: probing the ribosomal protein-Mdm2-p53 pathway. *Oncogene*, **29**, 4253–4260.
30. Ionescu,C.N., Origanti,S. and McAlear,M.A. (2004) The yeast rRNA biosynthesis factor Ebp2p is also required for efficient nuclear division. *Yeast*, **21**, 1219–1232.
31. Killian,A., Le Meur,N., Sesboüé,R., Bourguignon,J., Bougeard,G., Gautherot,J., Bastard,C., Frébourg,T. and Flaman,J.M. (2004) Inactivation of the RRB1-Pescadillo pathway involved in ribosome biogenesis induces chromosomal instability. *Oncogene*, **23**, 8597–8602.
32. Oeffinger,M., Fatica,A., Rout,M.P. and Tollervey,D. (2007) Yeast Rrp14p is required for ribosomal subunit synthesis and for correct positioning of the mitotic spindle during mitosis. *Nucleic Acids Res.*, **35**, 1354–1366.
33. Oeffinger,M. and Tollervey,D. (2003) Yeast Nop15p is an RNA-binding protein required for pre-rRNA processing and cytokinesis. *EMBO J.*, **22**, 6573–6583.
34. Cai,T., Aulds,J., Gill,T., Cerio,M. and Schmitt,M.E. (2002) The Saccharomyces cerevisiae RNase mitochondrial RNA processing is critical for cell cycle progression at the end of mitosis. *Genetics*, **161**, 1029–1042.
35. Gill,T., Aulds,J. and Schmitt,M.E. (2006) A specialized processing body that is temporally and asymmetrically regulated during the cell cycle in Saccharomyces cerevisiae. *J. Cell Biol.*, **173**, 35–45.
36. Gill,T., Cai,T., Aulds,J., Wierzbicki,S. and Schmitt,M.E. (2004) RNase MRP cleaves the CLB2 mRNA to promote cell cycle progression: novel method of mRNA degradation. *Mol. Cell. Biol.*, **24**, 945–953.
37. Okuda,M., Horn,H.F., Tarapore,P., Tokuyama,Y., Smulian,A.G., Chan,P.K., Knudsen,E.S., Hofmann,I.A., Snyder,J.D., Bove,K.E. *et al.* (2000) Nucleophosmin/B23 is a target of CDK2/cyclin E in centrosome duplication. *Cell*, **103**, 127–140.
38. Ugrinova,I., Monier,K., Ivaldi,C., Thiry,M., Storck,S., Mongelard,F. and Bouvet,P. (2007) Inactivation of nucleolin leads to nucleolar disruption, cell cycle arrest and defects in centrosome duplication. *BMC Mol. Biol.*, **8**, 66.

39. Piddubnyak,V., Rigou,P., Michel,L., Rain,J.C., Geneste,O., Wolkenstein,P., Vidaud,D., Hickman,J.A., Mauviel,A. and Poyet,J.L. (2007) Positive regulation of apoptosis by HCA66, a new Apaf-1 interacting protein, and its putative role in the physiopathology of NF1 microdeletion syndrome patients. *Cell Death Differ.*, **14**, 1222–1233.
40. Fant,X., Gnadt,N., Haren,L. and Merdes,A. (2009) Stability of the small gamma-tubulin complex requires HCA66, a protein of the centrosome and the nucleolus. *J. Cell Sci.*, **122**, 1134–1144.
41. Champion,E.A., Lane,B.H., Jackrel,M.E., Regan,L. and Baserga,S.J. (2008) A direct interaction between the Utp6 half-a-tetratricopeptide repeat domain and a specific peptide in Utp21 is essential for efficient pre-rRNA processing. *Mol. Cell. Biol.*, **28**, 6547–6556.
42. Dragon,F., Gallagher,J.E., Compagnone-Post,P.A., Mitchell,B.M., Porwancher,K.A., Wehner,K.A., Wormsley,S., Settlage,R.E., Shabanowitz,J., Osheim,Y. *et al.* (2002) A large nucleolar U3 ribonucleoprotein required for 18S ribosomal RNA biogenesis. *Nature*, **417**, 967–970.
43. Basi,G., Schmid,E. and Maundrell,K. (1993) TATA box mutations in the *Schizosaccharomyces pombe* nmt1 promoter affect transcription efficiency but not the transcription start point or thiamine repressibility. *Gene*, **123**, 131–136.
44. Voth,W.P., Jiang,Y.W. and Stillman,D.J. (2003) New 'marker swap' plasmids for converting selectable markers on budding yeast gene disruptions and plasmids. *Yeast*, **20**, 985–993.
45. Longtine,M.S., McKenzie,A. III, Demarini,D.J., Shah,N.G., Wach,A., Brachat,A., Philippsen,P. and Pringle,J.R. (1998) Additional modules for versatile and economical PCR-based gene deletion and modification in Saccharomyces cerevisiae. *Yeast*, **14**, 953–961.
46. Courtheoux,T., Gay,G., Gachet,Y. and Tournier,S. (2009) Ase1/Prc1-dependent spindle elongation corrects merotely during anaphase in fission yeast. *J. Cell Biol.*, **187**, 399–412.
47. Tournier,S., Gachet,Y., Buck,V., Hyams,J.S. and Millar,J.B. (2004) Disruption of astral microtubule contact with the cell cortex activates a Bub1, Bub3, and Mad3-dependent checkpoint in fission yeast. *Mol. Biol. Cell*, **15**, 3345–3356.
48. Gietz,D., St Jean,A., Woods,R.A. and Schiestl,R.H. (1992) Improved method for high efficiency transformation of intact yeast cells. *Nucleic Acids Res.*, **20**, 1425.
49. Gérus,M., Bonnart,C., Caizergues-Ferrer,M., Henry,Y. and Henras,A.K. (2010) Evolutionarily conserved function of RRP36 in early cleavages of the pre-rRNA and production of the 40S ribosomal subunit. *Mol. Cell. Biol.*, **30**, 1130–1144.
50. Henras,A., Henry,Y., Bousquet-Antonelli,C., Noaillac-Depeyre,J., Gélugne,J.P. and Caizergues-Ferrer,M. (1998) Nhp2p and Nop10p are essential for the function of H/ACA snoRNPs. *EMBO J.*, **17**, 7078–7090.
51. Haren,L., Remy,M.H., Bazin,I., Callebaut,I., Wright,M. and Merdes,A. (2006) NEDD1-dependent recruitment of the gamma-tubulin ring complex to the centrosome is necessary for centriole duplication and spindle assembly. *J. Cell Biol.*, **172**, 505–515.
52. Tollervey,D. (1987) A yeast small nuclear RNA is required for normal processing of pre-ribosomal RNA. *EMBO J.*, **6**, 4169–4175.
53. Pestov,D.G., Lapik,Y.R. and Lau,L.F. (2008) Assays for ribosomal RNA processing and ribosome assembly. *Curr. Protoc. Cell Biol.*, **39**, 22.11.1–22.11.16.
54. O'Donohue,M.F., Choesmel,V., Faubladier,M., Fichant,G. and Gleizes,P.E. (2010) Functional dichotomy of ribosomal proteins during the synthesis of mammalian 40S ribosomal subunits. *J. Cell Biol.*, **190**, 853–866.
55. Gallenberger,M., Meinel,D.M., Kroeber,M., Wegner,M., Milkereit,P., Bösl,M.R. and Tamm,E.R. (2011) Lack of WDR36 leads to preimplantation embryonic lethality in mice and delays the formation of small subunit ribosomal RNA in human cells in vitro. *Hum. Mol. Genet.*, **20**, 422–435.
56. Knop,M., Pereira,G., Geissler,S., Grein,K. and Schiebel,E. (1997) The spindle pole body component Spc97p interacts with the gamma-tubulin of Saccharomyces cerevisiae and functions in microtubule organization and spindle pole body duplication. *EMBO J.*, **16**, 1550–1564.
57. Raynaud-Messina,B. and Merdes,A. (2007) Gamma-tubulin complexes and microtubule organization. *Curr. Opin. Cell Biol.*, **19**, 24–30.
58. Chial,H.J. and Winey,M. (1999) Mechanisms of genetic instability revealed by analysis of yeast spindle pole body duplication. *Biol. Cell*, **91**, 439–450.
59. Jaspersen,S.L. and Winey,M. (2004) The budding yeast spindle pole body: structure, duplication, and function. *Annu. Rev. Cell Dev. Biol.*, **20**, 1–28.
60. Champion,E.A., Kundrat,L., Regan,L. and Baserga,S.J. (2009) A structural model for the HAT domain of Utp6 incorporating bioinformatics and genetics. *Protein Eng. Des. Sel.*, **22**, 431–439.
61. Preker,P.J. and Keller,W. (1998) The HAT helix, a repetitive motif implicated in RNA processing. *Trends Biochem. Sci.*, **23**, 15–16.
62. Savkur,R.S. and Olson,M.O. (1998) Preferential cleavage in pre-ribosomal RNA byprotein B23 endoribonuclease. *Nucleic Acids Res.*, **26**, 4508–4515.
63. Hoareau-Aveilla,C., Bonoli,M., Caizergues-Ferrer,M. and Henry,Y. (2006) hNaf1 is required for accumulation of human box H/ACA snoRNPs, scaRNPs, and telomerase. *RNA*, **12**, 832–840.